TEKNOFEST

AVIATION, SPACE AND TECHNOLOGY FESTIVAL

FIGHTER UAV COMPETITION

CRITICAL DESIGN REPORT

TEAM NAME: ASHWINCARRA

AUTHORS: JUSTIN EDWARDO, SAFIRA NADIA R., R.G.J. DIMAS P.H., ALBERTUS DAMAR W.P., MAULANA AKBAR I., AUFACLAV ZATU K.F., AND MUHAMMAD YUSUF H.

TABLE OF CONTENTS

1. BASE SYSTEM SUMMARY

1.1. System Description

The missions in the 2022 Teknofest Fighter UAV (Unmanned Aerial Vehicle) Competition demand that the UAV be capable of autonomous take-off and landing, autonomous target searching and locking, evading enemy locking, and also the kamikaze mission. The locking countermeasure consists of periodic evasive maneuver to make it more difficult to lock on to the UAV. Our autonomous locking program makes use of a lightweight deep learning approach while still meeting mission requirements. As a result, it runs on SBC with minimal resources and consumes less power. This program is an improved version of our previous technique, which is used at 2019 Teknofest Fighter UAV Competition.

The Ashwincarra UAV system is made up of numerous subsystems, including propulsion and actuators, power supply, image processing, autopilot and sensors, and also communication. In propulsion, a Brushless DC (BLDC) motor serves as the primary propulsion, with an Electronic Speed Controller (ESC) acting as a controller to drive the BLDC motor. Servos are used to control the control surfaces as actuators. The power source is a Lithium Polymer (Li-Po) battery with a total capacity of 16,000mAh and a configuration of 4 cells 2 parallels (4s2p) to deliver power to other subsystems, accompanied by a fuse to add safety features. Meanwhile, the autopilot hardware employs a flight controller, Global Positioning System (GPS), Light Detection and Ranging (LIDAR), and airspeed sensors to perform auto take-off, landing, and mission tasks, as well as offer a suitable attitude to the aircraft while flying. Image processing hardware, such as Session Border Controller (SBCs) and accelerators placed to UAVs, is used to support combat and kamikaze missions. All missions data are transmitted using the UAV's built-in communication system, which employs the Wi-Fi module for bidirectional connection between the UAV and the committee server with 5Ghz. Omnidirectional antenna is used for the telemetry through 433Mhz. First Ground Control Station (GCS) and Second GCS are the two methods used for the control station. The first Ground Control Station employs telemetry communication while running the Mission Planner software to setup, calibrate, and tune the UAV for optimal performance. The second ground control station communicates with the UAV through Wi-Fi. The second GCS is an interface that is used to communicate necessary data to the server and deliver commands to the UAV such as kamikaze mode, safe flight, autonomous take-off and landing, loiter, and escape.

Our aircraft has a pusher configuration and a v-tail as its empennage because it best meets our requirements. The pusher configuration allows us to place the camera in a fixed position at the front of the aircraft. A high-wing configuration provides the aircraft with high stability during locking missions. Additional missions, such as kamikaze, are carried out using the same software as the autonomous locking mission. As a result, our UAV carries out this mission during combat. The software directs the UAV to the coordinates of the ground target with a specific pitch angle, allowing the ground target to be seen from the camera.

1.2. System Final Performance Specifications

In the Fighter UAV competition, take-off, flight, landing, locking, and kamikaze mission, is performed autonomously. The basic system performances are developed by calculation and simulation. Using defined configuration, the performance reports based on the defined tasks is shown on Table 1.

Table 1. System performance specification

Technical Specifications		
Specifications	**Assumed**	**Actual**
Maximum Take-Off Weight (MTOW)	3.6kg	4kg
Cruise Speed	26m/s	22-26m/s
Cruising Altitude	100m	+100m
Stall Speed	9m/s	9m/s
Minimum Flight Time	20 minutes	20 minutes
Camera Resolution	5MP	8MP
Computer Capacity (with Accelerator)	4 TOPS	4 TOPS

2. ORGANIZATION SUMMARY

2.1. Team Organization

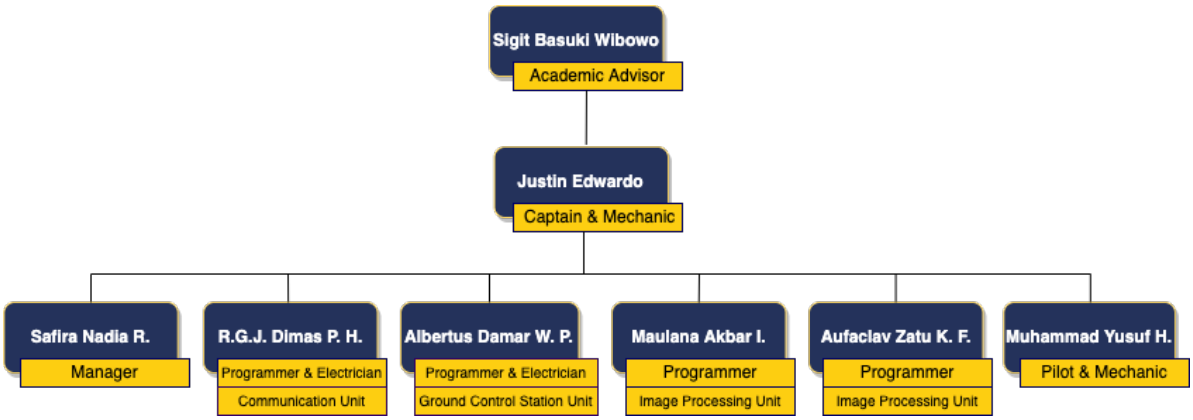

Figure 1. Team diagram and job description

In Figure 1, Ashwincarra team consists of seven people who are organized into numerous sections each with a distinct work description and an academic advisor. We work closely together to share ideas, set team goals, plan, and execute the project. To achieve the aim of the Fighter UAV Competition, each member performs their defined task based on their competence. The academic advisor evaluates the progress and provide technical advice. This team has eight roles, each with a different set of responsibilities.

- Team Captain : The team captain is responsible for directing the research project, providing strategic advice, and coordinating between divisions.
- Team Manager : The team manager is responsible for managing the team, starting from the timeline, finances, internal university administration, external competition administration, and correspondence.
- Electrician : The electrician is responsible for selecting and ensuring proper installation of all electronic components on the UAV.
- Mechanic : The mechanic is responsible for the UAV's design, analysis, material selection, and manufacture.
- Programmer : The programmer is responsible for developing the software used for missions involving Image Processing Unit and Communication Unit.

- Image Processing Unit : The image processing unit is responsible for the development of autonomous locking (object detection and tracking) and kamikaze software.
- Communication Unit : The Communication unit is responsible for coordinating communication between ground control and the UAV, as well as between the UAV and the pilot and the server. Additionally, the Communication division chooses the hardware, method, and develops software for the communication integration.

- Ground Control System (GCS) Unit : GCS unit is responsible for developing user interface of Ashwincarra's SGCS that has a specific task, which is to receive and transmit data from either the UAV or the server committee. GCS unit also responsible for manage Autopilot parameters.
- Pilot : The pilot who has completed basic remote pilot license course for professional, public, educational, and sport/recreational purpose with small Unmanned Aircraft System (sUAS) rating as described in the CASR part 107 is responsible for controlling the UAV while flying.

2.2. Timeline and Budget

2.2.1. Timeline

Since January 2022, research for the 2022 Teknofest Fighter UAV Competition has been underway. The process begins with data collection and adjustment, followed by the improvement of the UAV's design and component by adding new advancements based on the missions required. Figure 2 depicts the general plan for the 2022 Teknofest Fighter UAV Competition.

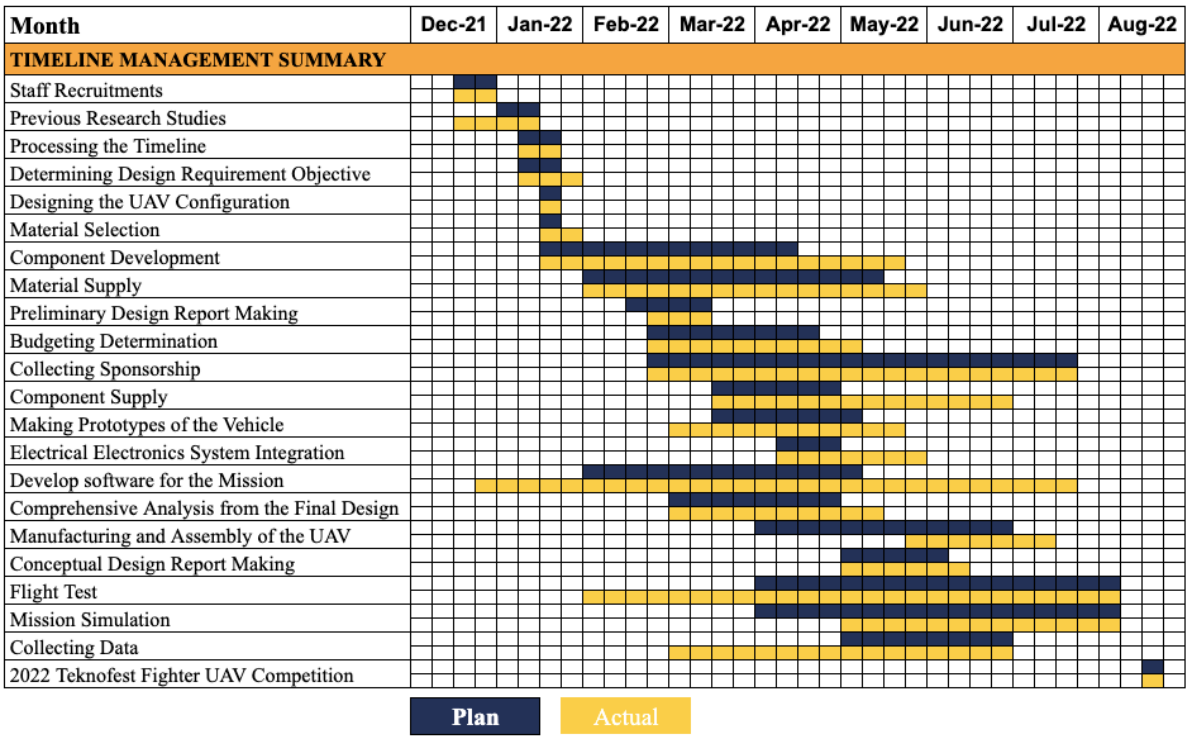

Figure 2. Timeline of Ashwincarra Team (Plan vs Actual)

2.2.2. Budget

The cost of producing the UAV and the system is an additional consideration. Ashwincarra UAV is designed to have adequate performance, the ability to complete the assigned missions, and with reasonably priced as shown in Table 2. Changes from the Preliminary Design Report (PDR) are made, including Wi-Fi components, battery capacity, ESC, and the addition of an airspeed sensor is explained in the next section.

Table 2. Plan and actual budget

Component	Specification	Qty	Plan	Actual
Flight Controller & GPS	Pixhawk 2.1 Cube Orange with GPS HERE 3	1	$503.55	$503.55
Wi-Fi ground	Ubiquiti Nanobeam AC Gen 2	1	$104.18	$108.35
Wi-Fi air	Ubiquiti Bullet AC	1	$103.83	$110.85
Remote	Futaba T14SG	1	$694.55	Available
Telemetry FC	3DR Radio Telemetry & Custom Antenna	1	$104.18	$118.07
Receiver	Futaba R7008SB 2.4GHz	1	$229.20	Available
LIDAR	GARMIN LIDAR V3 Lite	1	$337.16	Available
Motor	OS OMA 5010 810 KV Motor	1	$172.25	$172.25
ESC	Hobbywing 100A V4	1	$88.90	$88.90
Battery	ONBO 8,000mAh 25C	2	$115.57	$154.19
Propeller	APC 13x8inch	1	$6.95	$2.29
Power Module	Pixhawk Brick Powermodule	1	$45.15	$68.68
UBEC	Hobbywing UBEC 5V 3A	3	$32.30	$32.30
Step Up Module	XL6009	1	$3.47	$1.04
Fuse/Current Breaker	ANL Fuse 100A	1	$3.47	$2.43
Servo Aileron	EMAX ES3054	2	$28.20	$26.12
Servo Rudervator	EMAX ES08MD II	2	$20.56	$21.53
SBC	Raspberry Pi 4B 8GB	1	$225.03	$225.03
Detection Camera	Raspberry Pi V2 8MP	1	$34.38	$34.38
Accelerator	Coral USB Accelerator	1	$74.99	Available
Airspeed Sensor	PX4 Digital Airspeed Sensor	1	$68.68	$68.68
Carbon Fiber	3K 220gsm	4	$108.35	$108.35
Hardfoam	Density 20 kg/m^3	1	$24.31	$24.31
Epoxy Resin	Lycal 1011	1	$59.04	$59.04
Vacuum Bagging Film		1	$13.06	$13.06
Peel ply		4	$10.70	$10.70
Plywood	3mm	1	$2.78	$2.78
3D filament	ABS+	1	$17.99	$17.99
Monokote Film Covering		2	$18.75	$18.75
Balsa wood	3mm, 5mm, 8mm	12	$20.84	$20.84
Fibercloth (Fiberglass)	1.4oz (39,69 gram)	8	$55.56	$55.56
TOTAL			**$3,327.92**	**$2,070.00**

3. DETAILED DESIGN SUMMARY

3.1. Final System Architecture

First, the Wi-Fi radio, battery capacity, and Electronic Speed Controller are modified compared to previous Preliminary Design Report (PDR). Bullet AC is chosen as the Wi-Fi radio for the final update. Unlike the Bullet M5, the Bullet AC is capable of dual-band, the 2.4Ghz and 5Ghz frequencies. Bullet AC transfers data at 5GHz at speeds of 300+ Mbps, whilst the Bullet M5 only transfers at maximum speed of 100Mbps. This throughput enables the UAV to transmit data and video streaming with less latency. This modification is made because the AC series only communicates point-to-point with other AC series devices. Bullet AC is be able to communicate point-to-point with Nanobeam 5AC gen 2. For further information, Table 3 depicts the comparison between Bullet AC and Bullet M5.

Table 3. Comparison between Bullet AC and Bullet M5

Specification	Bullet AC	Bullet M5
Frequency	Dual Band (2.4Ghz and 5Ghz)	5Ghz
Data Transfer	300+ Mbps (for 5Ghz)	100+ Mbps
Power consumption	8W	6W
Output Power	158mW	316mW

Next, another change is made on the ONBO 6,200mAh 4s2p with a total capacity of 12,400mAh. This component is changed into ONBO 8,000mAh 4s2p with a total capacity of 16,000mAh due to provide more flight time. The unpredictability of the wind and the kamikaze mission need higher flight time to perform successfully. Next, the ESC 100A is chosen to replace ESC 80A. The reason is ESC 100A accepts a limit of 140A and the safe value for the ESC is 10-20% above the motor's maximum rating.

Figure 3 depicts the overall system architecture of the UAV and ground stations. The system architecture shows the components required for the Ashwincarra's UAV in detail to complete the mission successfully. The final architectural specification and components description are detailed in Table 4 through Table 8. The detailed components include the propulsion system, autopilot peripherals, sensors, and communication peripherals. To communicate between the UAV and the ground stations, two methods are used: first, for the connection between the aircraft and the first Ground Control System (GCS) uses telemetry module in frequency of 433MHz which receives data from the flight controller; and second, for the connection between the aircraft and the secondary GCS uses Radio Wi-Fi in frequency of 5GHz. The secondary GCS receives data from the Raspberry Pi like video streaming, altitude, and GPS coordinate.

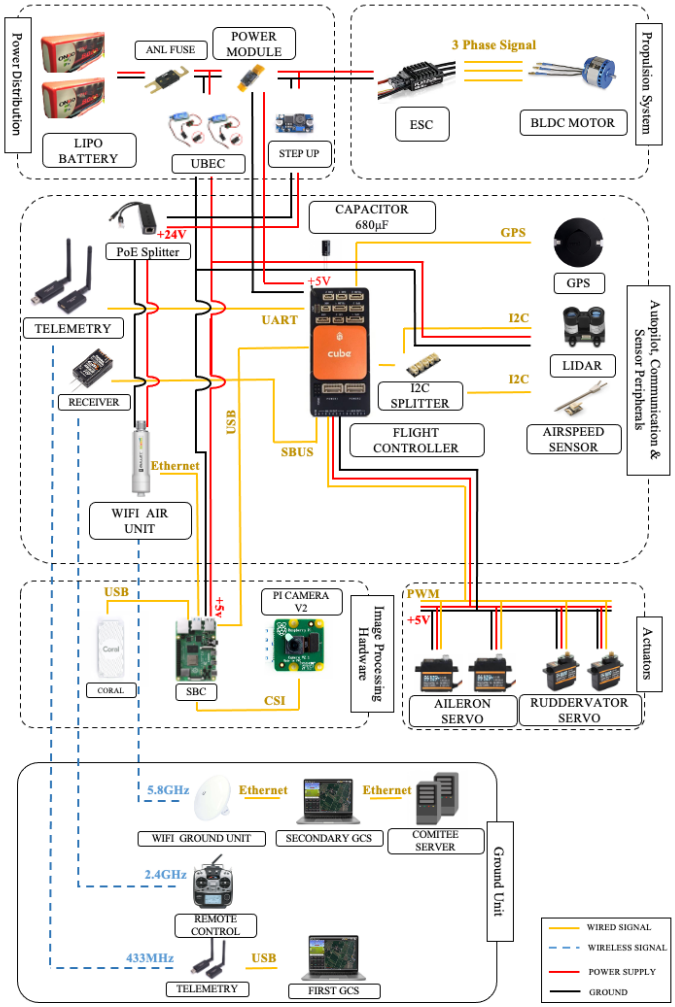

Figure 3. Final system architecture

Table 4. Power supply hardware

Power Supply Hardware		
Component	**Specification**	**Description**
Li-Po Battery	ONBO 8,000mAh 4s2p	Provides sufficient power for the propulsion and control systems to give sufficient flying time to complete the task.
Battery Eliminator Circuit	Hobbywing UBEC 3A, 5V, and 6V	A power regulator that reduces the 14.8V battery voltage of an aircraft to an acceptable level for other electrical systems.
Power Module	Pixhawk Brick Power Module	A method for providing Pixhawk Cube Orange with clean power from a Li-Po battery, as well as measuring current consumption and battery voltage.
Fuse	ANL Fuse 100A	To guard against overcurrent and short circuit for safety.
Step Up	XL6009	Utilized to supply power to the aircraft's Bullet M5 module.

Table 5. System of actuators and drives

Drive System & Actuators		
Components	**Specification**	**Description**
BLDC Motor	OS Motor OMA5010 810	The propulsion system's motor.
Electronic Speed Controller	Hobbywing 100A	The controller decides which motor wind must be powered to generate electricity in order for the motor to rotate.
Aileron Servos	EMAX ES3054	Actuator that delivers adequate torque for controlling ailerons.
Ruddervator Servos	EMAX 08MDII	Actuator that supplies adequate torque for controlling ruddervators.

Table 6. Autopilot and Sensors

Autopilot and Sensor Peripheral		
Component	**Specification**	**Description**
Flight Controller	Pixhawk Cube Orange	The primary control system and access hub of the UAV.
GPS Module	GPS Here 3	A function that provides exact aircraft location.
LIDAR	GARMIN LIDAR V3 Lite	A device sensing approach that uses pulsed laser light to measure ranges (varying distances) to earth.
Airspeed Sensor	PX4 Digital Airspeed Sensor	A stuff that provides the airspeed parameter, which is crucial for severe winds.

Table 7. Image processing hardware

Image Processing Hardware		
Components	**Specification**	**Description**
On-board Computer	Raspberry Pi 4B 8GB	Used in the image processing system to process picture data.
Accelerator	Google Coral USB Accelerator	An excellent hardware that enables Raspberry Pi to utilize the potential of artificial intelligence applications.
Camera	Raspberry Pi camera v2.1 8MP	The camera is used to create high-quality images to satisfy the requirements of the UAV target detection system.

Table 8. Communication peripherals

Communication Peripherals		
Components	**Specification**	**Description**
Wi-Fi Ground Unit	NanoBeam 5AC gen 2	Establishing a Wi-Fi connection network allows the Single Board Computer's data to be transmitted to the ground station.

Wi-Fi Air Unit	Bullet AC	Establishing a Wi-Fi communication network allows for the transmission of data from the on-board computer to the ground station.
Radio Receiver	Futaba R7008SB	The functions of their radio receivers are to obtain input signals from the remote-control transmitter.
Radio Transmitter	Futaba T15SG	Their functionalities are radio control receiver to obtain input signals from the remote-control transmitter.
Telemetry	Frequency 433MHz Band with 20dBm (100mW)	It has the ability to transmit data, and from the ground control station we view live data such as GPS location overlap on a map, system voltage, direction, and waypoint navigation.

3.2. Subsystems Summary

3.2.1. Power and Propulsion System

In the Preliminary Design Report (PDR), the battery is a Li-Po ONBO battery with a capacity of 6,200mAh for each battery and a 4s2p configuration for a total capacity of 12,400mAh. In the final system, a Li-Po ONBO battery with a capacity change of 8,000mAh for each battery and a 4s2p configuration is used for the battery's total capacity is 16,000mAh. Previously, the calculation for selecting a battery when powered by 183.52Wh and cruising at constant throttle resulted in a total flight time of 21.2 minutes. However, considering the uncertain conditions and the additional kamikaze missions that requires high dive maneuvers, the final calculation at 16,000mAh capacity with additional propulsion power is to fly with 90-100% throttle cruise. Based on Equation 1, the total time is 19.8 minutes when powered by 236,8Wh battery. With this estimated time, the vehicle still has nearly 5 minutes to wait for all participants to fly and complete the mission. Table 9 shows estimated power consumption during the cruising condition and full throttle.

Table 9. Estimated power consumption during the cruising condition and full throttle

Component	Power (Watt)	Power (Watt)
SBC	5	5
Servo	5	5
FC + GPS + Telemetry + Receiver	2	2
Propulsion Cruise	500 (cruise only)	694 (throttle 90-100 %)
Wi-Fi	8	8
LIDAR	1	1
Camera	1	1
Estimated Power Consumption	**522**	**714**

This equation corresponds to the final power consumption depicted in Equation 1.

$$tflight = \frac{BampRating\ x\ 14.8}{Pconsumption}\ x\ 60\ min = \frac{16\ x\ 14.8}{714}\ x\ 60\ min = 19.8\ \text{min} \quad (1)$$

Where tflight denotes the flight time of the UAV, BampRating denotes the battery storage ampere rating, and Pconsumption denotes the UAV's total power consumption.

To calculate the propulsion system, two methods are used: manual calculation and software calculation. These calculations are performed to discover the ESC safe for motor maximum rating, flight time, electric power, and thrust to weight of the UAV. The calculation for the safety ESC is shown in Equation 2. Figure 4 depicts the result of electric power and thrust to weight using eCalc software.

Figure 4. Propulsion calculation

The UAV's brushless motor OS OMA5010 810KV with a 13x8-inch propeller produces 3.7kg of thrust with a maximum current output of 62A. The motor requires a constant current output of 62A and a burst current of 70-80A at maximum performance. The safe ESC value is 20% greater than the motor's maximum rating. As a result, an ESC with a constant current output of 100A is chosen in the propulsion system. Table 10 provides a comparison of ESC 80A and ESC 100A.

$$ESC = Max.Motor\ Current + (Max.Motor\ Current\ x\ 20\%) \quad (2)$$

$$= 80 + (80\ x\ 20\%) = 96A$$

Table 10. Comparison between ESC Platinum 100A and Platinum 80A

Parameter	**Model**	
	Platinum 100 A	**Platinum 80 A**
Input	3-6s Li-Po	
Cont./Burst Current	100A/140A	80A/100A
Weight/Size	77x35x21mm/104g	84.29x38.2x20.44mm/96.5g

For the control surface, two types of servos are used EMAX ES3054 for ailerons and EMAX ES08MD II for ruddervators. According to section 8.1.1.3 Control Surface Force, 20.63N force on aileron and 15.58N force on ruddervator, the EMAX ES3054 has a stall torque of 3.5kg.cm and an operating speed of 0.13 sec/60°, making it ideal for ailerons with high lifts. The EMAX ES08MD II's stall torque is 2.0kg.cm, and its operating speed is 0.1sec/60°.

3.2.2. Autopilot and Sensor Peripherals

The UAV's flight controller is a Pixhawk 2 Cube Orange. The flight controller is the component that allows a UAV to fly autonomously. The Pixhawk 2 Cube Orange has a triple redundant Inertial Measurement Unit (IMU). GPS is used for UAV navigation to position the UAV and as a gyro on the UAV in addition to being a navigation system. The UAV's GPS coordinates are Here 3 Hex. Furthermore, the PX4 Digital Airspeed sensor is used to transfer UAV speed data more accurately by measuring fluid flow in the pitot tube. The pressure is measured by an attached device is fluid flow dependent and is used to calculate velocity. Pitot tube is utilized in anemometer to measure the velocity of air in the wind and over UAV. The sensor used to transfer altitude data is the Garmin LIDAR V3. This sensor is useful for assisting the UAV when landing and performing the kamikaze mission.

3.2.3. Communication Peripherals

There are three methods for communicating between the UAV and the ground station as mentioned in Figure 5, which is explained in the following section.

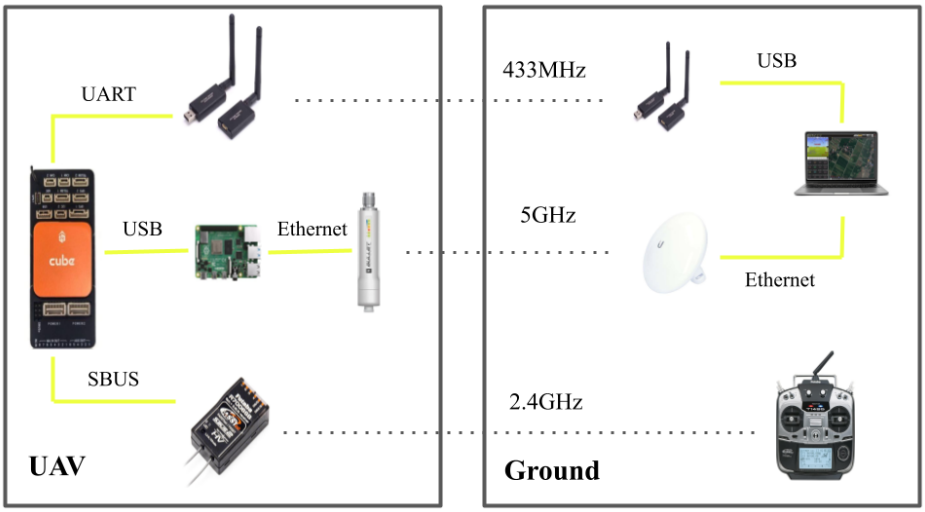

Figure 5. Communication peripherals

3.2.3.1. Telemetry Communications

To transfer UAV Telemetry data to ground control stations, it is used effectively over 800m and works in sync with the Pixhawk 2 Cube Orange flight control in UAV, as well as the transfer speeds. The telemetry module has a 433MHz frequency and an omnidirectional antenna. The telemetry package contains data such as UAV latitude and longitude, altitude, level angle, orientation angle, bank angle, air speed, ground speed, and flight mode to Mission Planner software.

3.2.3.2. Wi-Fi Communication

The GPS data, lock, and image data are transferred from the on-board computer to the ground station. We use the Nanobeam 5AC Gen 2 for the ground station and the Bullet AC for the aircraft. Nanobeam 5AC Gen 2 supports 5GHz frequency and airMAX technology, with a data transfer rate of more than 450Mbps and a range of up to 15km, as well as significant latency performance. The Bullet AC supports dual-band 2.4Ghz and 5Ghz frequencies. Bullet AC supports airMAX AC technology. Table 11 shows the specification of Wi-Fi.

Table 11. Wi-Fi specification

Specification	Bullet AC	Nanobeam 5AC gen 2
Frequency	Dual Band (2.4Ghz and 5Ghz)	5Ghz
Data Transfer	300+ Mbps (for 5Ghz)	450+ Mbps
Power consumption	8W	8.5W
Output Power	158mW	316mW
Technology	airMAX AC	airMAX AC

3.2.3.3. Pilot Communication

During a competition, pilot communication is used to determine whether or not to assume control of an Unmanned Aerial Vehicle (UAV) in an emergency. Futaba T15SG for the transmitter and R7008SB for the receiver with 2.4GHz frequency are used for this communication.

3.2.4. Image Processing Hardware

The Raspberry Pi 4 on-board computer assists the aircraft in completing its mission (data transfer, locking, and video streaming via camera). The Coral USB Accelerator adds an Edge TPU coprocessor to the Raspberry Pi simply by plugging it into an USB port. The Raspberry Pi camera version 2.1 records H.264 video at 1080p resolution at a frame rate of 30 Frames Per Second (FPS). The Raspberry Pi camera has changed from version 1.3 with resolution 5MP to version 2.1 with resolution 8MP.

3.3. Aircraft Performance Summary

Participating the 2022 TEKNOFEST Fighter UAV Competition, the aircraft that is used for the missions is designed by our team. This decision is made to maximize the performance and compatibility for the aircraft itself following the Fighter UAV missions. Calculations and considerations are mentioned below in this chapter.

3.3.1. Basic Aircraft Design Calculation

Wing loading and power loading are the most important design considerations for UAVs because they influence aerodynamic performance and propulsion selection (Raymer, 2018). The acquired wing loading, power loading, and CLmax are portrayed in Figure 6 based on the Design Requirements and Objectives (DRO) and calculation over requirements (considering take-off, cruise, and stall speed requirements (Roskam, 2003).

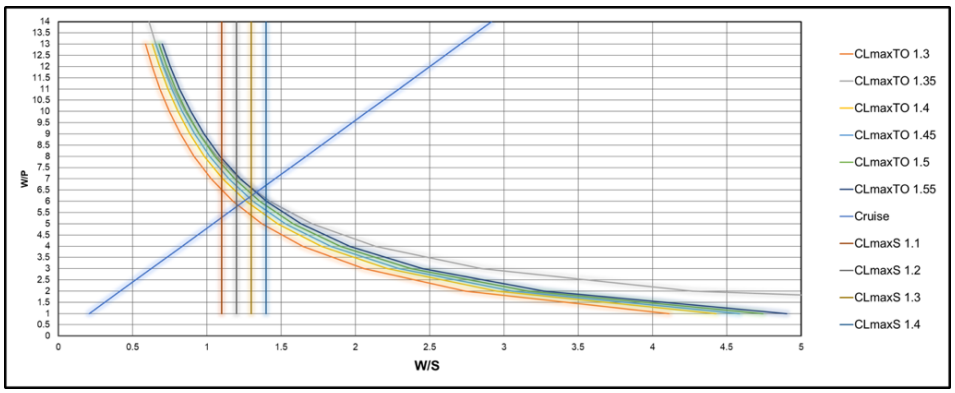

Figure 6. Wing Loading vs Power Loading diagram

Based on the performance considerations presented in Figure 6, a preliminary determination of wing area and power requirement are made, as well as the proper airfoil selection based on CLmaxTO and CLmaxS, as shown in Table 12.

Table 12. Preliminary determination based on wing loading and power loading requirement

Wing Loading	Power Loading	MTOW	Wing Area	Power Req.	CL_{maxTO}	CL_{maxS}
1.299lb/ft^2 (6.344kg/m^2)	6.3lb/hp (260.95W/kg)	7.93lb (3.6kg)	6.107ft^2 (0.567m^2)	1.258hp (938.090W)	1.45	1.3

3.3.2. Airfoil Selection

Based on the conditions around the aircraft, cruising speed, and CLmax requirements (listed in Table 6), a low Reynolds Number Airfoil suits best for our mission. (Selig *et al.*, 1995). As a result, some comparisons exist between Selig/Donovan Low Reynolds Number Airfoils with (t/c) % of around 10%, such as S4062-095-87, SD7032-099-88, SD7084, SD7090, and SD8040.

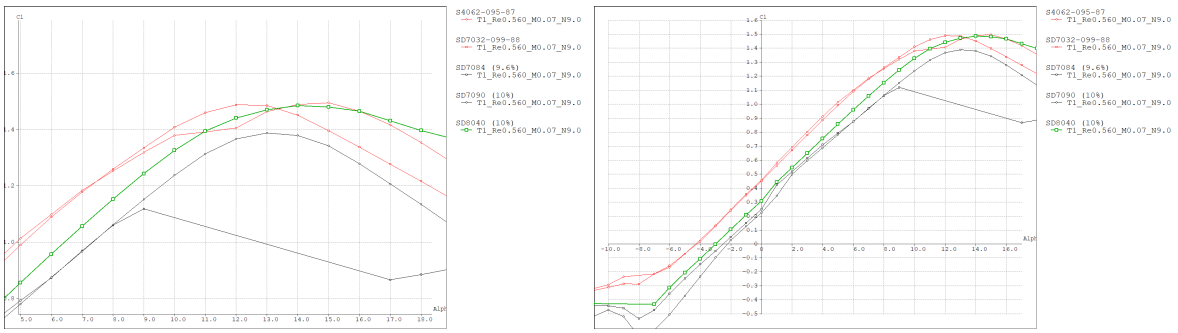

(a) (b)

Figure 7. CL vs AoA (α) graph comparison between airfoils

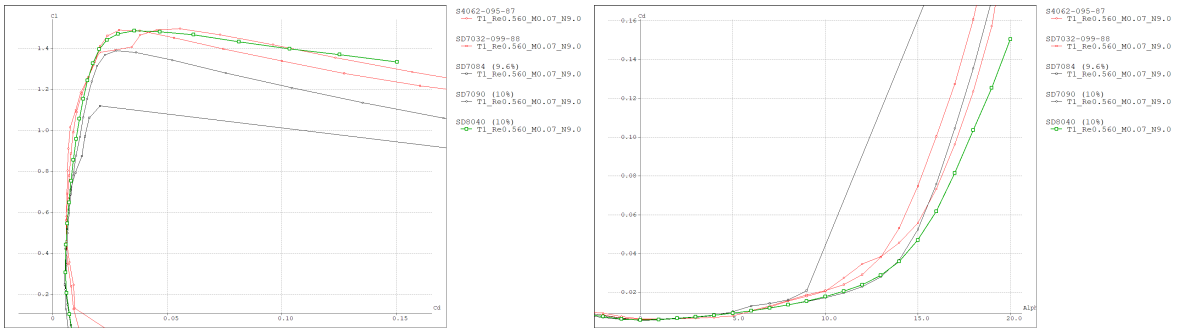

(a) (b)

Figure 8. (a) CL vs CD graph comparison between airfoils; (b) CD vs AoA (α) graph comparison between airfoils

As seen in Figure 7, S4062-095-87, SD7032-099-88, and SD8040 are met CLmaxTO requirements above 1.45, but only SD8040 meets CLmaxS requirements above 1.3. Then, by comparing CL/CD as aerodynamic efficiency of the airfoil (Figure 8 (a)), SD8040 has the highest of CL/CD. Figure 8 (b) reveals that the SD8040 has the lowest CD over AoA (α) compared to other airfoils. From considerations explained in this section, the SD8040 is chosen as our main airfoil.

3.3.3. Empennage Selection

Due to some advantages, choosing v-tail configuration as our aircraft empennage is highly recommended after considering mission requirements as mentioned in the Preliminary Design Report (PDR), such as being stable enough to lock onto enemy while also being agile enough to maneuver quickly. The implementation of this empennage configuration will necessitate less elevator deflection, reduce tail buffeting, have less interference drag due to the use of only two stabilizers, and provide superior maneuverability (Snorri Gudmundsson, 2014). Choosing 110° as the angle between each v-tail stabilizer and 35° dihedral angle for each stabilizer as a reference to level ground surface is considered because it provides superior directional stability to prevent Dutch Roll (Sanchez-Carmona and Cuerno-Rejado, 2019).

3.3.4. Overall Lift, Drag, and Pressure Distribution

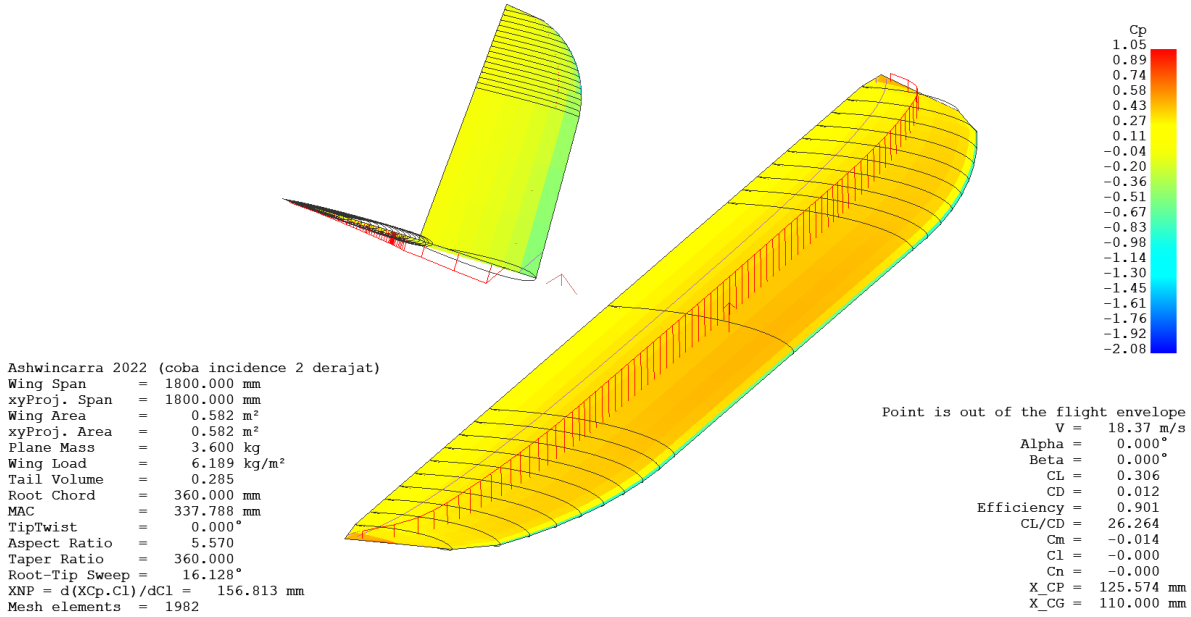

Figure 9. The analysis after having incidence angle of 2°.

XFLR5 software is used to analyze initial lift, drag, and pressure distribution around the wing using the Type 2 (Fixed Lift) Vortex Lattice Method (T2-VLM). Our aircraft has an incidence angle of about 2° after analyzing and discussing our preliminary design. Other than having the highest CL/CD at 2° of initial alpha (α), this decision is based on gaining higher lift, compensating for a low thrust to weight ratio, and gaining more flight time at a lower throttle in cruising mode. The red line above the wing indicates the distribution of lift and pressure over the wing's surface. At the new initial 0° angle of attack, the resulting CL and CL/CD are 0.306 and 26.264 respectively. This pressure distribution is used to design wing spars that need to hold the most pressure when cruising at 0° AoA.

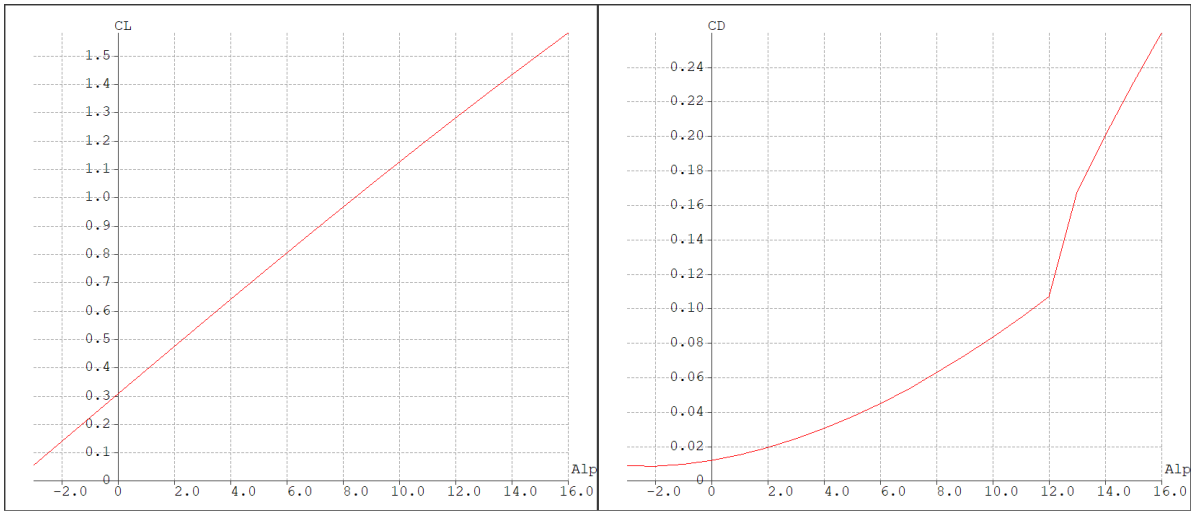

Figure 10. CL vs AoA (α) and CD vs AoA (α) graph based on XFLR5 analysis

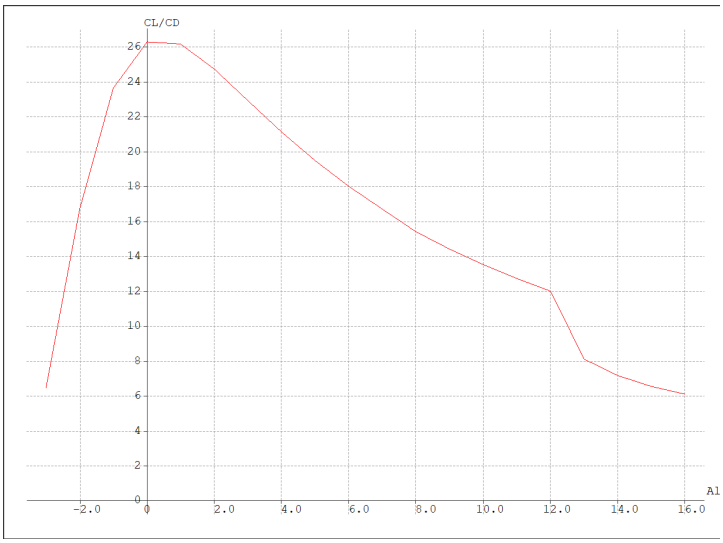

Figure 11. CL/CD vs AoA (α) graph based on XFLR5 analysis

Based on Figures 10 and 11, we examine the CL and CD graphs in relation to the change in the plane's angle of attack. Figure 10 portrays the magnitude of the new lift and drag coefficients following the modification described earlier. Figure 11 demonstrates that, based on the greatest CL/CD, the angle of attack of 0 degrees yields the highest efficiency.

3.3.5. Control Surface Sizing

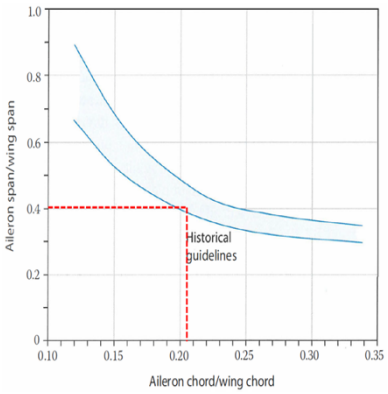

This section explains the sizing of control surfaces such as aileron and ruddervator. Standard control surface dimensions are based on the aileron guideline dimensions shown in Figure 12. As indicated by the red lines in the figure, the aileron and ruddervator is designed using span and chord control surfaces derived from the meeting point of the historical guidelines.

Figure 12. Control surface sizing graph

3.3.6. Stability Analysis

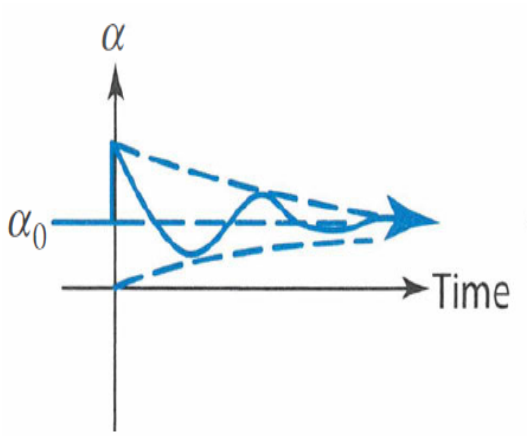

Figure 13. Stable and lightly damped stability

Before embarking on a flight, determining the aircraft's center of gravity is one of the most crucial decisions that must be made. Our aircraft must have sufficient stability while locking onto an enemy aircraft and returning as quickly as possible to its initial 0° AoA (α) while pitching up and down (see Figure 13) (Raymer, 2018). Based from X_NP and X_CG value on Figure 9, in order to have good longitudinal stability in front of the neutral point, we determine the static margin between 5% and 15%.

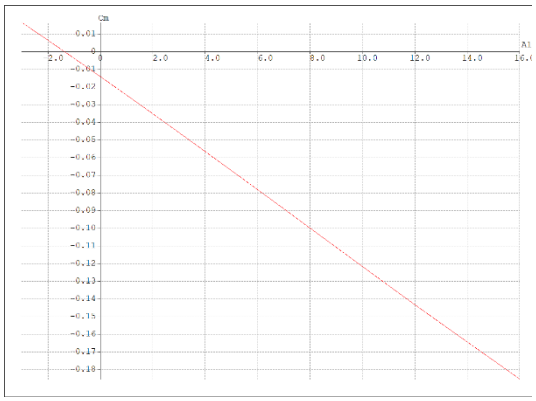

Figure 14. CM vs AoA (α) graph based on XFLR5 analysis

X_CG within 110mm of the leading edge of the wing is selected and analyzed in XFLR5. The negative slope of the graph CM versus AoA (α) indicates a stable aircraft (Snorri Gudmundsson, 2014). Negative moment at 0° AoA indicates positive static and dynamic aircraft stability. Based on the static margin formula, the static margin for our aircraft is approximately 13%, which meets our initial requirement for the aircraft.

3.4. 3D Design of Aircraft

In Figure 15, an exploded view provides a summary of the placement of several of the competition's primary components. Figure 16 shows a technical drawings and general dimensions indicating the size of some aircraft components. Lastly in Figure 17, the design has been rendered in three dimensions using the software Autodesk Inventor 2022. The three-dimensional model is an illustration of the aforementioned calculations and descriptions.

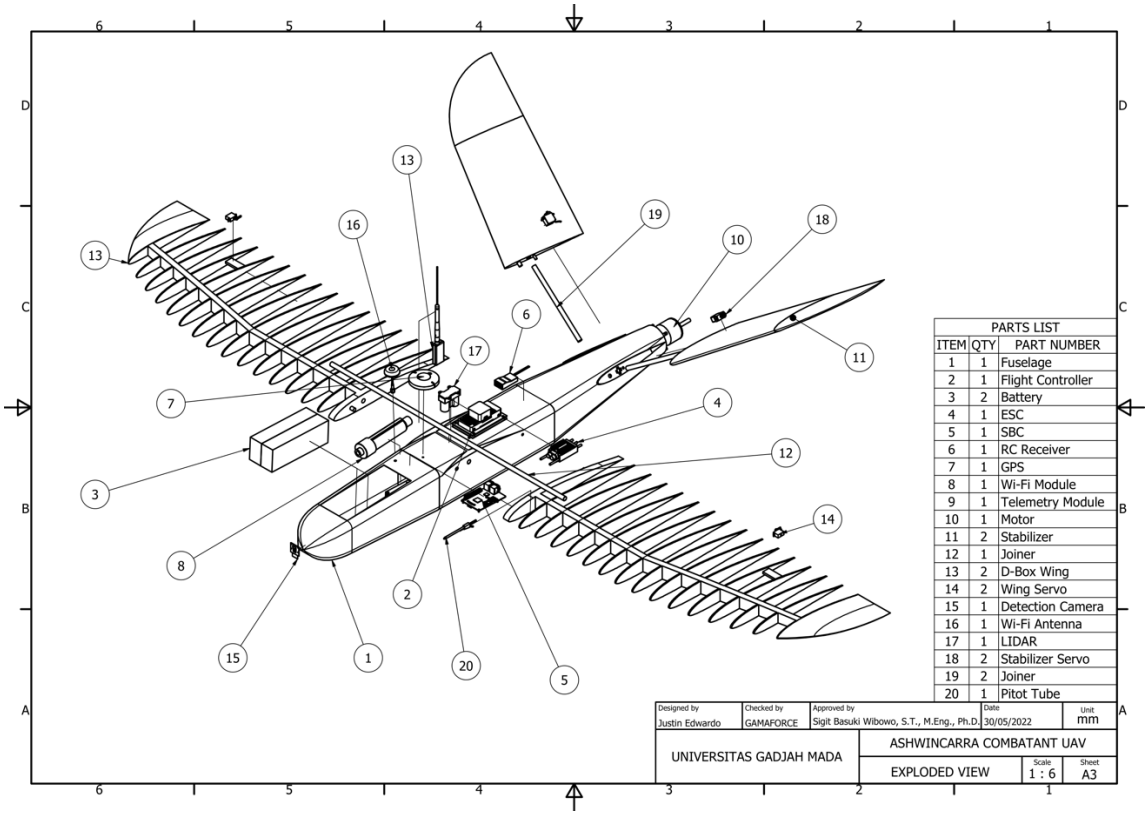

Figure 15. Exploded view of the UAV

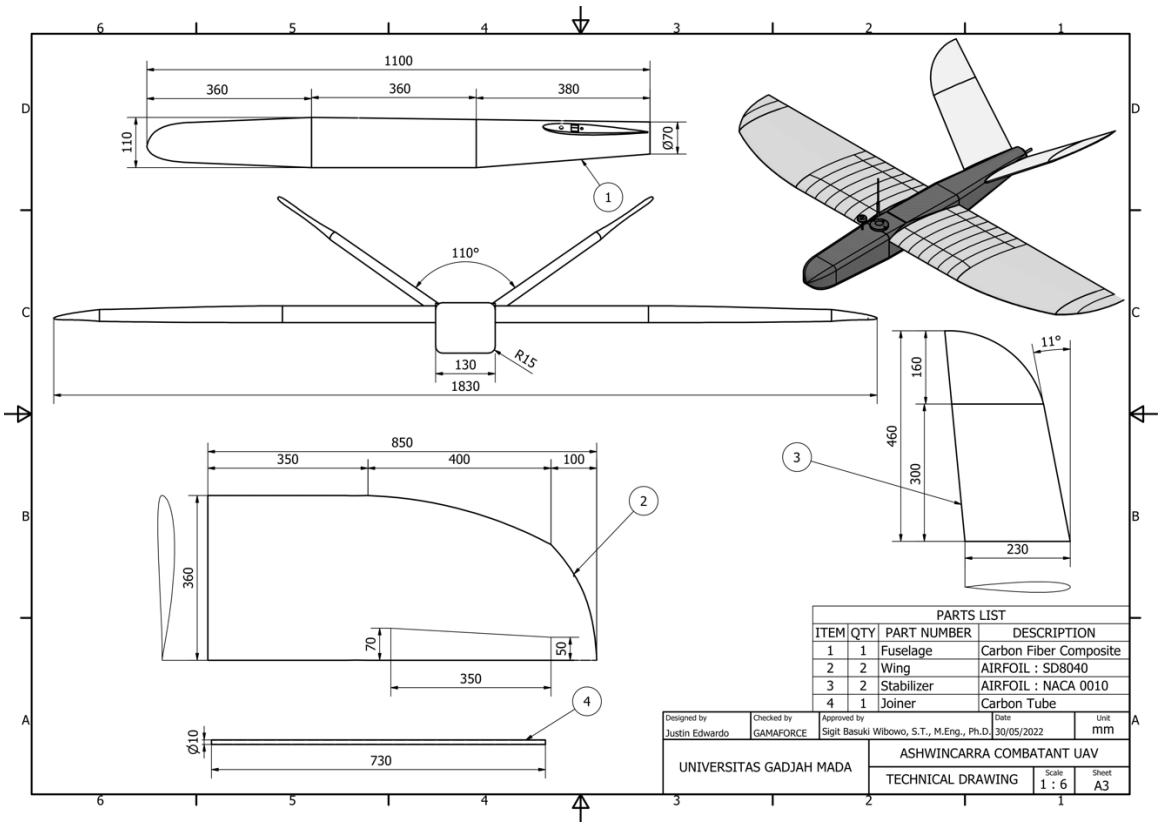

Figure 16. Technical drawing of the UAV

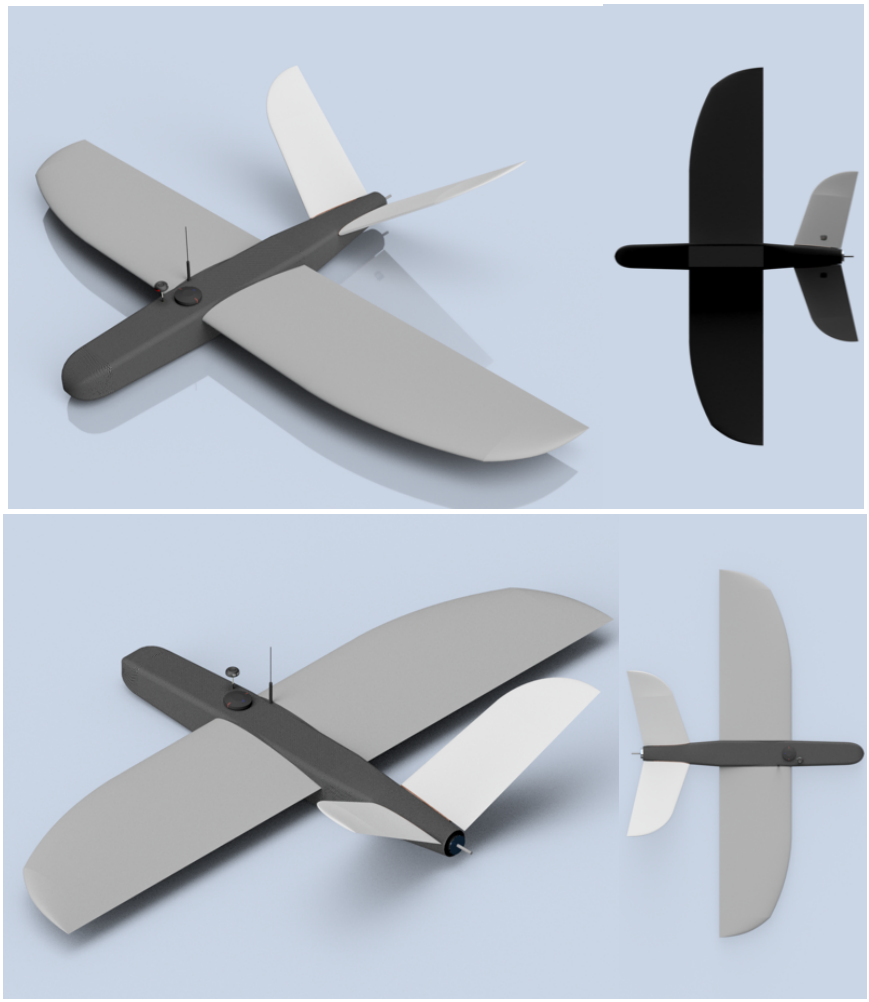

Figure 17. 3D design of the UAV

3.5. Aircraft Weight Distribution

This section describes the weight distribution of each component used for competition which is determined according to the center of gravity point. As mentioned previously in Section 3.3.6 Stability Analysis, the center of gravity is located 470mm from the nose of the aircraft toward the rear of the aircraft or 110mm from the leading edge of the wing.

Table 13. Weight distribution

Component	Mass (kg)	Weight (N)	X (mm)	Moment (Nmm)
Motor	0.31	3.038	-625	-1898.75
ESC	0.132	1.2936	-120	-155.232
Battery	1.47	14.406	270	3889.62
Propeller	0.029	0.2842	-660	-187.572
Step Up Module	0.005	0.049	140	6.86
UBEC	0.005	0.049	140	6.86
PMD	0.028	0.2744	140	38.416
Fuse/Current Breaker	0.01	0.098	140	13.72
SBC	0.047	0.4606	140	64.484
Detection Camera	0.004	0.0392	460	18.032
Accelerator	0.034	0.3332	140	46.648

Servo Aileron	0.034	0.3332	-100	-33.32
Servo Ruddervator	0.024	0.2352	-510	-119.952
GPS	0.049	0.4802	97	46.5794
Flight Controller	0.097	0.9506	10	9.506
Wi-Fi Air	0.123	1.2054	150	180.81
Telemetry FC	0.014	0.1372	-90	-12.348
Receiver	0.012	0.1176	-170	-19.992
LIDAR	0.022	0.2156	-150	-32.34
Pitot tube	0.01	0.098	30	2.94
AWG Cable	0.05	0.49	-300	-147
Wings Joiner	0.019	0.1862	18	3.3516
Wings	0.87	8.526	-10	-85.26
Propeller Nut	0.005	0.049	-660	-32.34
Stabilizers Joiner	0.016	0.1568	-465.888	-73.0512384
Stabilizers	0.248	2.4304	-522.825	-1270.67388
M8 wingnuts for Wing	0.008	0.0784	56	4.3904
M5 wingnuts for Wing	0.002	0.0196	-150	-2.94
M5 washers for Wing	0.002	0.0196	-150	-2.94
M8 washer for Wing	0.004	0.0392	56	2.1952
M8 wingnuts for Stabilizer	0.008	0.0784	-432.02	-33.870368
M5 wingnuts for Stabilizer	0.002	0.0196	-588.35	-11.53166
M5 washer for Stabilizer	0.002	0.0196	-588.35	-11.53166
M8 washer for Stabilizer	0.004	0.0392	-432.02	-16.935184
Fuselage	0.297	2.9106	-100	-291.06
Mounting camera	0.04	0.392	455	178.36
Moment Total				**74.1326096**

4. AUTONOMOUS MISSIONS

To meet the requirements of the mission, software including autonomous lockdown and kamikaze mission is developed. The program operates on the on-board computer of the UAV, which controls the UAV's flight by processing data from our secondary GCS and image data from the camera. The software is made using the Python on the Robot Operating System (ROS), a framework that provides libraries and tools for the development of robotic software **(**Quigley, Morgan, et al., 2009**)**. ROS enables the execution of software with numerous nodes that communicate with one another. ROS contains a MAVROS package that allows communication between the computer and the flight controller. With this package, the computer receives data from the flight controller and controls the UAV utilizing the package's functionalities. The mission software is designed so the aircraft decides and follows the missions assigned as shown in Figure 18.

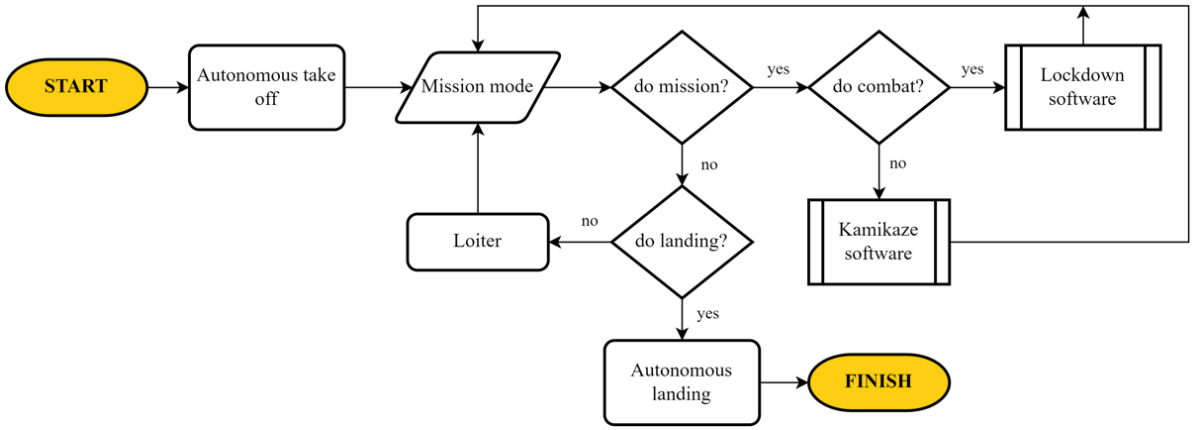

Figure 18. Autonomous mission software block diagram

The UAV take-off autonomously. UAVs carry out missions according to instructions received for lockdown or kamikaze. There is also a loiter mode which is prepared as a safe flight mode. The next section describes the software for each mission.

4.1. Autonomous Lockdown

The Autonomous Lockdown software aims to lock the UAV that has been defined as a target in image capture and perform autonomous tracking. Figure 19 illustrates how the lockdown software works.

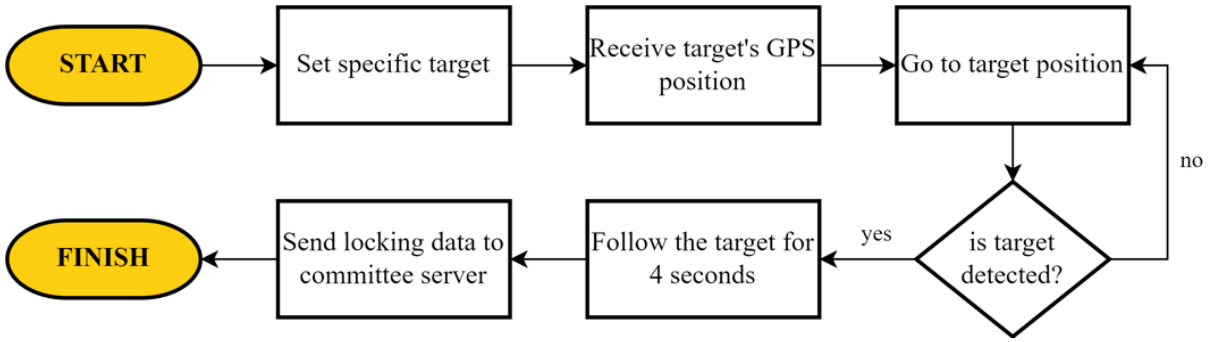

Figure 19. Autonomous lockdown software block diagram

The entire process begins by defining a lockdown target. The UAV autonomously tracks the target using GPS coordinates provided from the server. If the target distance is close and visible from the camera, the detection module detects the target and return the target's bounding box as the output. The position of target in the image frame is transmitted to the GCS and routed to the committee server. In addition, the position of target is also utilized to help the primary control system (which is based on GPS tracking) by adjusting the heading of the UAV based on the target position in the image frame. This method is referred to as "centering" assist control. According to mission requirements, the UAV requires to follow the target for four seconds.

The autonomous lockdown software created by our team consists basically of two sub-software, **Object Detection Software** and **Tracking Control Software**. The method used in each sub-software is described in the next section.

4.1.1. Object Detection Software

4.1.1.1. Object Detection Algorithm

The shape of the fixed-wing UAV varied and is diverse. This makes both standard image processing techniques and conventional machine learning by hand-crafted feature extraction inappropriate for this software purpose. To fulfill the mission requirement of detecting other UAVs, we apply a deep learning method. There are numerous alternatives for object detection methods based on deep learning (Kim, Sung and Park, 2020), the Faster Recurrent Convolutional Neural Network (Faster R-CNN) (Ren *et al.*, 2017), You Only Look Once (YOLO) (Redmon *et al.*, 2016), and Single Shot Detector (SSD) object detection methods (Liu *et al*., 2016). The comparison results between the methods are described in Table 14.

Table 14. Comparison of detection algorithms

Detection Algorithm	Advantages	Disadvantages
Faster R-CNN	Detects objects well in general, but with less precision than YOLO.	Provides the lowest FPS and slowest method.
YOLO	Provides the highest precision, generally best at recognizing objects.	Not provide the highest FPS on standard architecture.
SSD	Delivers the best FPS among other models, with an architecture designed for mobile devices.	Provides lower precision but sufficient (0.9). Generally, failure happens on small objects.

From this comparison, the method that produces the best precision is YOLO, while SSD provides the best FPS. Faster R-CNN provides lower precision than YOLO and lowest FPS. The SSD architecture being compared on that research is MobileNet. This architecture belongs to the mobile architecture family designed for devices with low computing resources. Considering the power limitations of the UAV, we chose to use the mobile architecture on the SSD method, so that it runs on power-efficient devices. In addition, the precision given by the SSD method is above 0.9.

SSD-MobileDets is chosen as the model architecture. This design is chosen because it outperforms a number of alternative architectures, including MobileNet and MnasFPN (Xiong *et al.*, 2021). This architecture is available in the SSD-Lite variant, one of the most popular lightweight detection heads (Sandler *et al.*, 2018). In section 8.2.3.1 Autonomous Lockdown Test, the performance of the used object detection algorithm is presented.

4.1.1.2. Object Tracking Algorithm

Object detection algorithms don't provide perfection in capturing object's movement on all frames. Therefore, we add an object tracking algorithm that works to help track objects when the detection algorithm fails. We compare several objects tracking algorithms, including Centroid Tracker (Rosebrock, Adrian, 2018), Channel and Spatial Reliability Tracking (CSRT) (Lukežič *et al.*, 2018), Multiple Instance Learning (MIL) (Babenko *et al.*, 2009), and Kernelized Correlation Filter (KCF) (Henriques *et al.*, 2015) for tracking UAV movement from video. We observe the tracking precision, frame rate, and stability. As a result, the CSRT and MIL

algorithms provide the best tracking precision but give a frame rate drop below 10 FPS. The centroid tracking algorithm is very fast in processing, there is no significant FPS reduction with this method. The drawback is that this method is not good at predicting the position of objects.

The most suitable algorithm is the KCF tracker, it tracks objects with sufficient precision and gives a stable FPS at around 30 FPS. This tracking method is an implementation of Henriques *et al.* (2015) extended to KCF with the color name feature, which is available in OpenCV library. This method divides the tracking process into blocks consisting of target region, patch appearance representation, training, model update, and detection. Figure 20 depicts the block diagram of the KCF tracker, where target region is the output bounding-box of the object detection method.

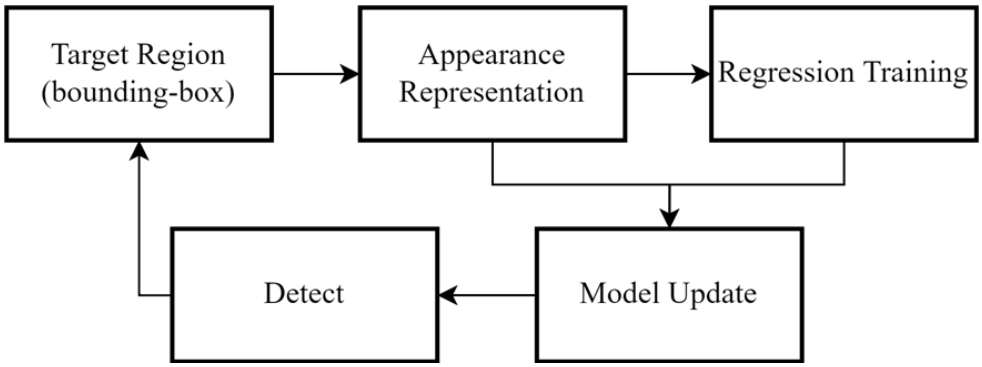

Figure 20. The KCF tracker block diagram

4.1.1.3. Object Detection Model Development

The object detection model training begins with data acquisition. The data consists of images of various types of UAVs captured using the camera on the UAV following behind with a forward-facing viewing angle. The raw image obtained is 640x480 pixels in size with variations in lighting and various sides of the UAV. To add variety, data augmentation is performed by flipping, rotating, scaling, and variating image color. Image variations ensure the robustness and accuracy of the object detection model. The dataset sampled for training consists of ~5.000 images. Figure 21 shows an example of the training dataset.

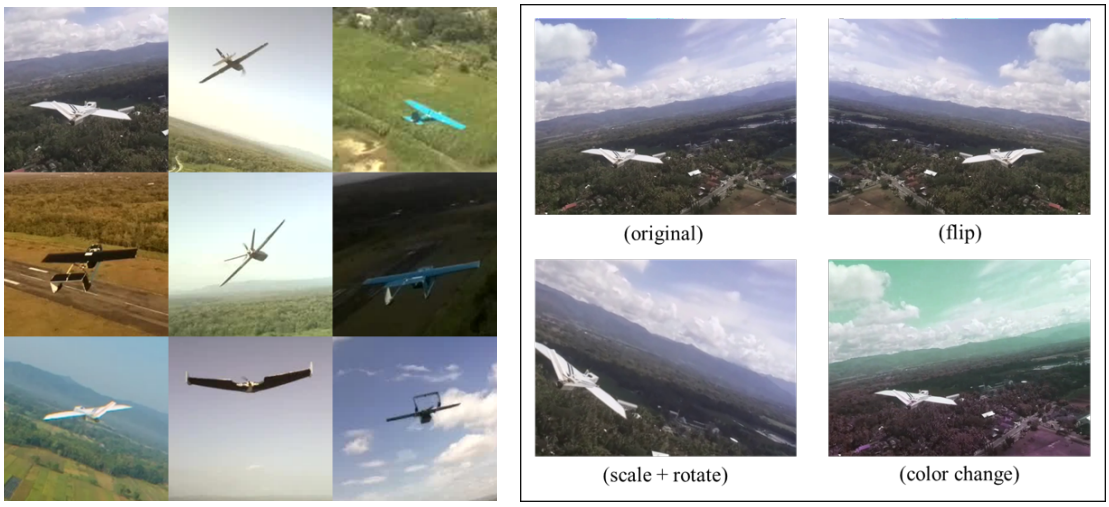

(a) (b)

Figure 21. (a) UAV type variation in dataset, (b) Data augmentation

Due to the limited computing speed of the on-board computer, the model is quantized to allow for real-time execution. Quantization considerably reduces the computational requirements for model inference while maintaining precision (Wu *et al.*, 2016).

4.1.2. Tracking Control Software

4.1.2.1. GPS-based Tracking Control Software

Utilizing the GPS data of other participants from the committee's server, a GPS-based tracking control mechanism is selected as the primary tracking method for the UAV being tracked. By tracking the GPS position, our UAV detects a predefined target even if the target is not visible to the camera. This method also prevents control mistakes if the vision-based method is used as the primary method towards error detection. Vision-based tracking control is still used, but only as an assistant to the main method.

Due to the delay of the GPS data collected from the committee's server, a data processing approach is required to estimate the most recent target position. The secondary GCS performs GPS data processing as a background process, as detailed in section 5.2.2. GPS Data Processing. Predicted target GPS data is delivered from the GCS to the UAV's on-board computer. The data is then pushed to the flight controller as waypoint using one of the MAVROS functions.

4.1.2.2. Centering Assist Control

Centering control is intended to increase the accuracy of tracking control, so that the UAV maintains its position directly facing the target when locking. This method generally changes the direction of the UAV with the image as input. Figure 22 depicts the detected object's position within the frame as input for the software.

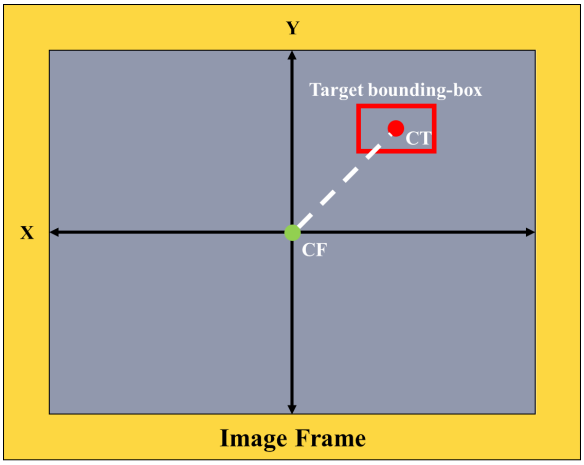

Figure 22. Target position in the image frame

This method is designed to maintain the Center of Target (CT) point in the Center of the Frame (CF). CT consists of 2 axis, center of target X and Y (*Xt*, *Yt*). *Xt* and *Yt* are used to find the target deviation on each X and Y axis to CF, with the Equation 3 and 4.

$$devX = \frac{Xt}{FW} - 0.5 \quad (3)$$

$$devY = \frac{Yt}{FH} - 0.5 \quad (4)$$

where, devX = deviation X, devY = deviation Y, FH = Frame Height, and FW = Frame Width. The value of the target deviation is between -0.5 to 0.5.

The deviation value becomes the input of a PID controller in order to assign Pulse Width Modulation (PWM) values to the control surface and perform adjustments to the UAV's roll and pitch. devX determines the PWM value to change the roll, while devY changes the pitch. This control method is executed together with the main control and takes priority because it gives direct input to the control surface in the "AUTO" mode of the main control. Similar to the main control, this control also employs MAVROS packages to send PWM values to the actuator.

4.2. Kamikaze Mission

In addition to the main mission, there are kamikaze missions which are performed during the same round. If the UAV is assigned a kamikaze mission, the software generates waypoints for diving and scanning the ground target. Figure 23 depicts the operation of our kamikaze software. Control software to perform a kamikaze mission requires at least three waypoints (P_1, P_2, and P_3) as shown in Figure 24.

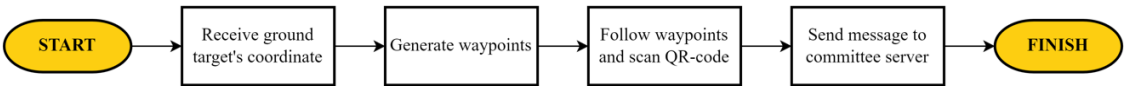

Figure 23. Kamikaze mission software block diagram

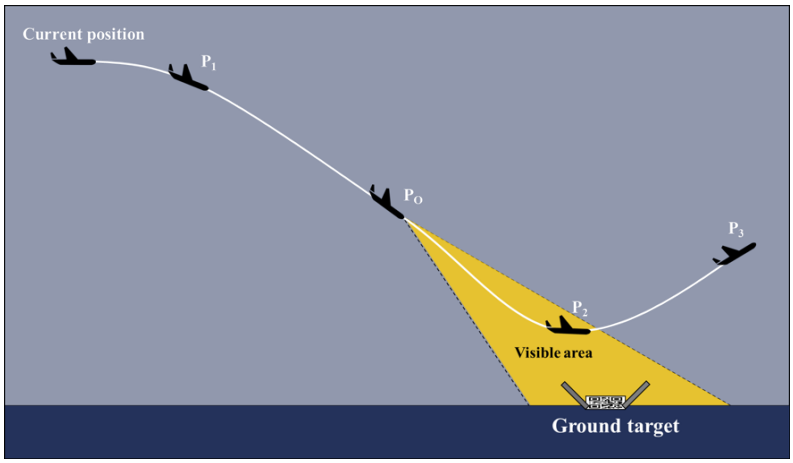

Figure 24. Waypoints for kamikaze mission

Current position is the position when the UAV gets the command to start the mission. Waypoints P_1, P_2, and P_3 are defined which form a straight line that crosses the coordinates of the target ground. The P_1 and P_2 are designed so that the UAV provides the maximum pitch down angle within safety limits. Between the two waypoints above the QR-code reading software is performed. P_o is the optimum position for the UAV to get a message from the QR-code and send it to the committee's server. After reaching P_2, the UAV begins to climb to increase its altitude at P_3. If the UAV enters the route to scan the QR-code, the QR-code encoding software is executed. There is an online open source Pyzbar in a Python package developed by L. Hudson (2022) is used for this task.

5. GROUND STATION AND COMMUNICATION

5.1 Communication System

The communication system is responsible for communication between ground control and the UAV, as well as between the UAV and the pilot. There are three types of communications in the system: communication between the pilot and the UAV, between the first ground control stations and the UAV, and between the second ground control stations. The frequency and power for the communication system are shown in Table 15.

Table 15. Communication system

Usage	Frequency	Power
Radio Control	2.4Ghz	100 mW
Telemetry	433Mhz	100 mW
Wi-Fi	5Ghz	125 mW

5.1.1 Communication between pilot and UAV

The receiver is used to control the UAV by the pilot using a radio controller for communication between the aircraft and the pilot. The radio controller is a Futaba T14SG, and the receiver is a R7008SB connected to the SBUS input pin on the autopilot. Futaba's spread spectrum offers maximum protection from same-channel interference, the best interference suppression available, a wide bandwidth for increased security, high-speed frequency hopping, and a range of over 2000m. The transmitter and receiver alternate between channels every 8ms. During the brief period of occupying any one channel, all signal conflicts or interruptions are avoided. The Futaba transmitter has an SBUS2 port that is used to connect various telemetry sensors. The radio controller, which programmed to control a fixed-wing aircraft. It communicates via the FASSTest protocol, has up to 18 channels, and is compatible with all telemetry sensor units.

5.1.2. Communications between First Ground Control Stations and UAV

The first ground control station is used to communicate between the UAV and Mission Planner. MAVlink protocol, a messaging protocol for communicating with drones that is extremely lightweight is utilized for point-to-point data transmission between UAV and ground station. The frequency for this communication is 433MHz with the MAVLink protocol. Extensible Markup Language (XML) files are used to define messages. Each XML file defines the message set that a specific MAVLink system supports. Most ground control stations and autopilots implement the reference message set defined in.xml. Telemetry data are transmitted using a multicast design, whereas mission protocols and parameterized protocols, which change the system configuration and require delivery point-to-point with retransmission.

5.1.3. Communications between Second Ground Control Stations and UAV

Wi-Fi is used for communication between UAVs and Secondary Ground Control Stations. The Wi-Fi connection will be point-to-point between the UAV and the ground control. The UAV's radio Wi-Fi uses Bullet AC and Nanobeam 5AC gen2 for the ground stations. Bullet AC is configured as an access point, while Nanobeam 5AC gen 2 is configured as a station point. Its communication frequency is 5GHz. To activate the airMAX AC technology, the channel size is set to 80MHz for the Nanobeam 5AC gen 2 and Bullet AC. This communication

is capable of transferring data at a throughput of 327.60Mbps over a distance of 500m with low latency. The NanoBeam 5AC Gen 2 is intended for use as a long-distance internet bridge or connection. Figure 25 depicts the throughput capacity of Wi-Fi.

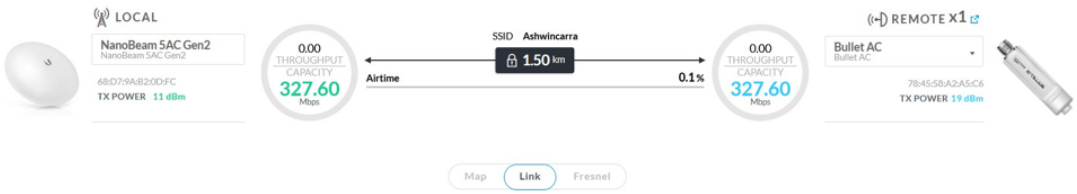

Figure 25. Point-to-point Wi-Fi

5.2. GCS-Committee Server

5.2.1. Communication Method

The ground control station communicates with the server in order to transmit Ashwincarra's UAV data and to receive UAV data from other participants. Data received by the ground station and transferred to the server, such as UAV coordinate, altitude, locking status, and position of the locking area. The GCS computer is linked to the server network through an Ethernet cable for this purpose. The HyperText Transfer Protocol (HTTP) is utilized for communication between the server and UAV.

5.2.2. GPS Data Processing

The GPS data of other participants is processed first, as it is utilized for tracking purposes. Considering the delay in data delivery, GPS data processing aims to provide the latest GPS position estimates. The target's GPS coordinates are show in Figure 26 below.

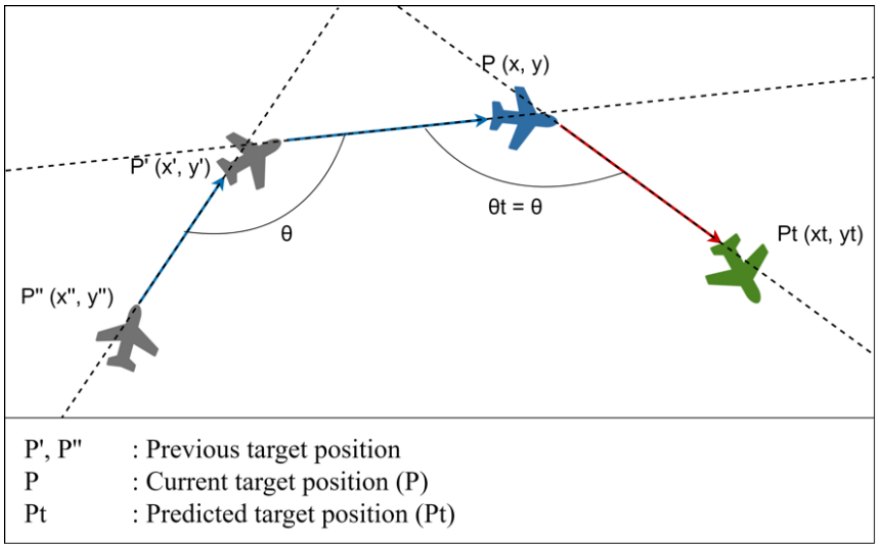

Figure 26. GPS data estimation

To predict the current position of the target based on two previous positions (P', P") and the current data received (P). From these three positions, the target flight direction is obtained in the form of bearing (in degrees) between P" to P' and P' to P using the spherical equation in Equation 5.

$$bearing = \arctan 2\left(\sin \Delta\lambda \cdot \cos \varphi_2,\ \cos \varphi_1 \cdot \sin \varphi_2 - \sin \varphi_1 \cdot \cos \varphi_2 \cdot \cos \Delta\lambda\right) \quad (5)$$

Where, (φ_1, λ_1) = start point in radians, (φ_2, λ_2) = end point in radians. With that equation, we get bearings between P'' to P' and P' to P. From two bearings obtained, the angle of change in the target's flight direction is calculated using Equation 6.

$$\theta = bearing_2 - bearing_1 \qquad (6)$$

The next target direction change (θt) is predicted to be equal to θ, so the target bearing, $bearing_t = bearing_2 + \theta$. In addition to predicting the target's flight direction, it is necessary to predict the distance traveled to determine the current target position. The target position changes from P'' to P takes 2 seconds (because data from the server is received every 1 second). The average speed for the previous 2 seconds (v) multiplied by the data delay is the predicted distance traveled. The altitude at P is utilized as the target altitude since the centering control accommodates altitude deviations.

6. USER INTERFACE DESIGN

In the fighter UAV competition, an UAV with GCS applying full duplex communication with the autopilot system is required. UAV equipped with GCS has the capability to complete missions, set PID, read sensors, and change flight modes, among other capabilities, while the autopilot functions. To meet the requirements of the competition, we employ two distinct control station approaches, namely Mission Planner as the primary software and the Secondary Ashwincarra GCS as the secondary control center.

6.1. Mission Planner

Figure 27. User interface of first Ashwincarra's ground control stations

Mission Planner displays data from Ardupilot, which is one of the most widely used open-source GCS software. Mission Planner monitors the UAV via telemetry data, such as diagnostic information from the flight control sensor, the live map location of the craft during mission planning, and manages the UAV's safety feature. The Mission Planner is installed on a laptop running Windows as shown in Figure 27. Table 16 provides a description of Mission Planner User Interface (UI).

Table 16. Description of Mission Planner UI

No	Mission Planner	Description
1.	Roll Navigation	It shows roll in degree.
2.	Pitch Navigation	It shows pitch in degree.
3.	RSSI Strength	Indicator telemetry signal strength.
4.	Quick Status	It consists of column and row of selected parameters.
5.	Mode Flight	Show current flight mode.
6.	Map	Show real time position of UAV.
7.	Connection Port	To establish connection between Mission Planner and Autopilot.

6.2. Secondary Ashwincarra Ground Control Station

The Ashwincarra Team developed the user interface for Secondary GCS. It is responsible for receiving and transmitting data from either the UAV or the server committee. The interface was developed in Python using the Tkinter Package due of its simplicity, adaptability, and ease of integration with other systems. The interface is separated into four sections, which are described in greater detail below. A locking image, a map indicating the location of the opposing UAV, a control panel, and a data display are included. Figure 28 depicts the interface's appearance. Figure 29 shows the workflow of the secondary GCS.

Figure 28. User interface of secondary Ashwincarra's ground control station

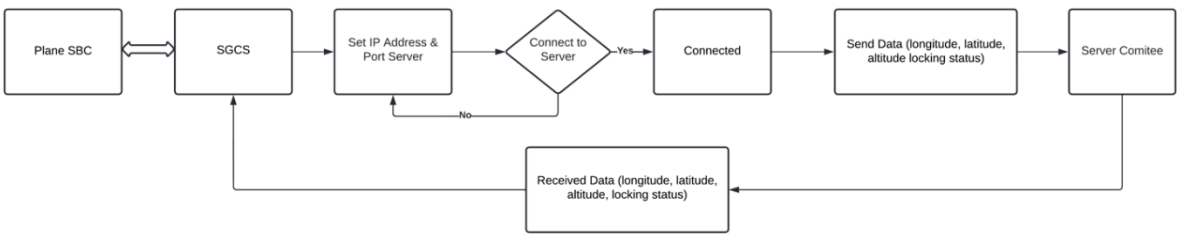

Figure 29. Secondary GCS software process diagram

6.2.1. Locking Image

In this section, the locking result is transmitted in real-time and displayed on the interface. This feature is utilized to communicate the locking status to the committee server. OpenCV is selected as our library of functions for real-time image processing. OpenCV offers built-in techniques and functions for working with Computer Vision to perform image processing. Figure 30 depicts the detection test result and Table 17 describes the locking image.

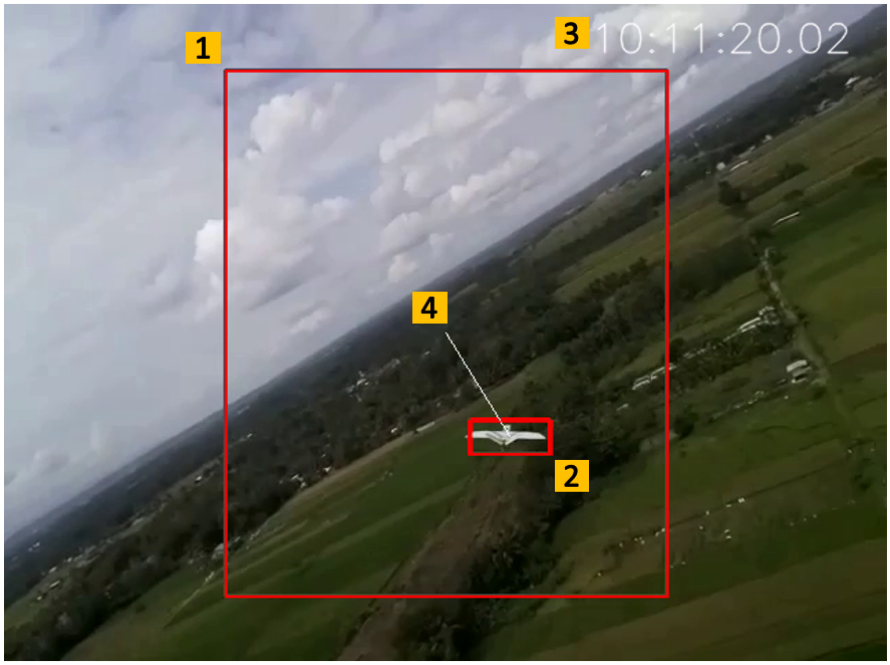

Figure 30. Locking result on Secondary Ashwincarra Ground Control Station

Table 17. Description of Locking Image

No.	Locking Image	Description
1.	Locking Boundaries	The area that must contain the target area.
2.	Target Bounding Box	It displays the target area.
3.	Server Time	It presents synchronous server time.
4.	Projection Line	Line between the center of target and center of frame.

6.2.2. Flight Radar

During the flight mission, the flight computer transmits GPS data which is going to be marked on this image using the Maps Static Api. For display map, flight radar uses a simple GPS data visualization. The UAV's location is displayed on a display map utilizing GPS data as an icon converted to pixels. Thus, the location and route of the UAV are monitored in real time via the interface. Figure 31 depicts the result of the UAV mark and Table 18 describes the flight radar.

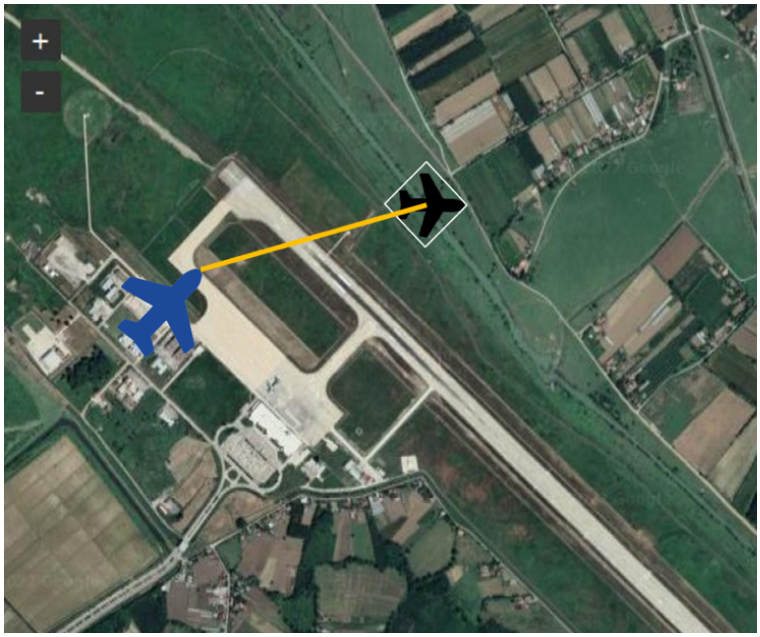

Figure 31. UAV mark

Table 18. Description of flight radar

No.	Flight Radar	Description
1.	Opponent Icon	The icon moves dynamically based on GPS and also identifying opponents Id.
2.	Map	Screen displays the vehicle track as it moves.

6.2.3. Control Panel

Figure 32. Control panel

The control panel contains button widgets for three primary missions: kamikaze, combat, and safe mode. The control buttons cause the program to carry out a specific mission based on the button's label. It is provided with a button widget that has the ability to activate the flight mode program that is embedded in the SBC for the control section. By including a button, the user interface has more interactive elements (see Figure 32). Table 19 provides a description of the functionality of each button.

Table 19. Description of control panel

No.	Control	Description
1.	Kamikaze	Activate the UAV's Kamikaze mission.
2.	Combat	The UAV begins to lock on to the enemy.
3.	Safe fly	The UAV flies to maintain altitude and position.
4.	Take-off	Increase the altitude to ascend higher.
5.	Land	Reduce the altitude to ground level.
6.	Escape	Avoid the enemies locking.

6.2.4. Data Display

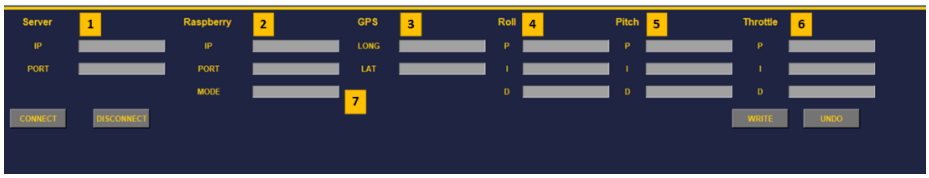

Figure 33. Data display

Not only transmitted to the server, the data also requests that aircraft-specific data be displayed on this screen. It is required to display flight mode, arm condition, communication address, lock status, and GPS location. Additionally, MAVLink telemetry messages sent between the autopilot and the ground station are logged. The roll, yaw, and pitch PID has been added to the SGCS with the ability to tune the PID parameter to change gradually during UAV tracking maneuvers. Figure 33 depicts the data display interface, whereas Table 20 describes each data display part.

Table 20. Description of data display

No.	Display	Description
1.	Server IP and Port	To retrieve data from server.
2.	Raspberry Pi IP and Port	To link the SGCS to the Raspberry Pi.
3.	GPS	Display the UAV's longitude and latitude data.
4.	PID Roll	To configure roll PID.
5.	PID Pitch	To configure pitch PID.
6.	PID Throttle	To configure throttle PID.
7.	Mission Mode	To determine which mode occurred on UAV.

7. AIRCRAFT INTEGRATION

7.1. Structural Integration

7.1.1. Wing Integration

The spar section of the wings is constructed from balsa wood reinforced with carbon and kevlar. D-Box construction is used to construct the wing of the aircraft in order to provide the strength necessary to maneuver at 2G+ loads (more than two times its weight) while keeping the structure light enough for the aircraft to fly as intended. Load force is a measure which determines the acceleration produced by Earth’s gravity on an object or individual. The spar is manufactured by hand-cutting balsa wood using a template provided by the wing's technical drawing. The technical sketch is also needed to ensure that the wing ribs are correctly aligned and glued.

Figure 34. Main spar construction

Figure 35. Complete ribs construction

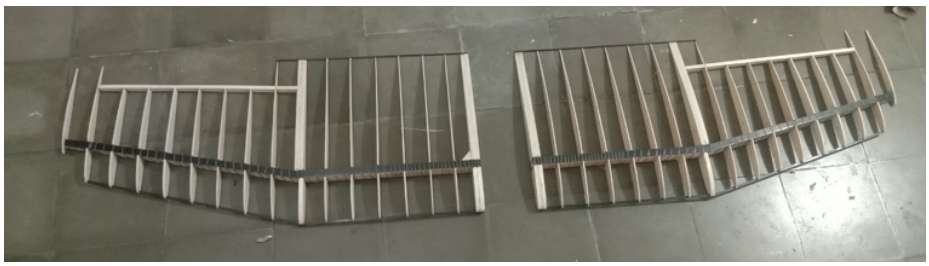

Figure 36. Frontal ribs without the D-Box structure

At the leading edge, trailing edge, and wing rib border, the wing is reinforced with carbon strip. In addition, a D-Box structure is utilized to provide additional strength and maintain the airfoil shape at the wing's leading edge. Balsa wood and fiberglass were used to construct the D-Box structure of the prototype aircraft. The final design's D-Box structure is made of carbon fiber.

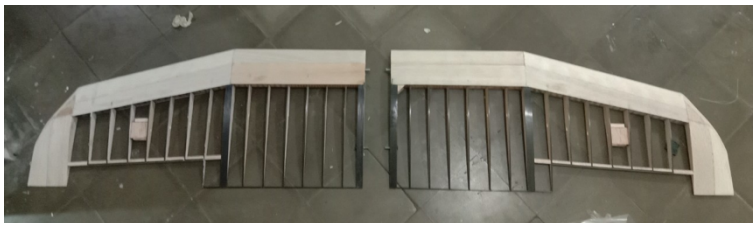

Figure 37. Complete prototype wing

The wing's frame is coated with a monokote film covering. Due to a lack of material in the form of carbon fiber sheets during the prototype manufacturing process, the wing used in the final design differs slightly from the wing shown in Figure 37 and 38 (a). As a mid-section wing spar, a 10-mm-diameter carbon tube is installed through the fuselage to connect both wings. It also prevents dislocation of the wings, particularly rotation about the lateral axis.

(a)

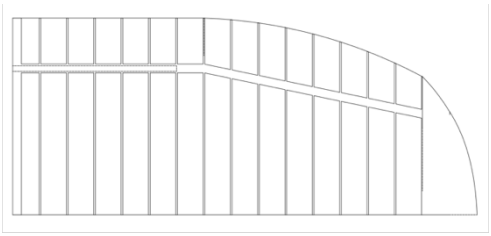

(b)

Figure 38. (a) Complete prototype wing with monokote, (b) Final design plan

7.1.2. Fuselage

Figure 39. Utilization of lantor soric coremat and outlets

Due to a lack of the primary material, carbon fiber composite, the fuselage of the prototype of our aircraft is constructed from fiber glass composite material. In addition to the D-Box method described previously, the final aircraft also utilizes a carbon fiber composite in the competition. The fuselage has a length of 1100mm and is designed for pusher aircraft. In Figure 39, the composite material is strengthened by the addition of lantor soric coremat to increase stiffness in sections of the aircraft such as the stabilizer and wing area. There are also outlets at the rear of the aircraft for air exchange caused by a component with a high temperature inside the fuselage, as well as an inlet at the front of the aircraft. Following the 3D-printed part for the detection camera, the front of the fuselage is cut.

7.1.3. Empennage

To increase the material's strength, stabilizers are created with a hard foam core and two layers of fiberglass composite 1.4oz laminated in different fiber directions as shown in Figure 40. Along the center of pressure each stabilizer, a carbon strip with a thickness of approximately 3mm is added to withstand the stabilizer's transverse load. As a joiner between the stabilizer and the fuselage, a 10mm carbon tube is utilized. To secure each component, a bolt-and-nut system is utilized.

Figure 40. The final form of the manufactured stabilizer

7.2. Mechanical Integration

7.2.1. Antenna tracker

In order to get reliable communication between GCS and aircraft computer, antenna tracker is used to direct Wi-Fi antennas that have directional radiation pattern. The antenna tracker used in the system consists of two RDS3115 servos as actuators and a microcontroller to control its movement. The antenna tracker system is powered by a 4s1p 14.8v Li-Po battery configuration. The battery is connected to a voltage regulator to provide a voltage that matches the specifications of the servo and a microcontroller used. Plywood is used for mounting structures on servos and a microcontroller due to its availability and easy to manufacture. This structure is made using a laser cutting technique with a CAD drawing that has been made in CAD software. Figure 41 shows the tracker configuration.

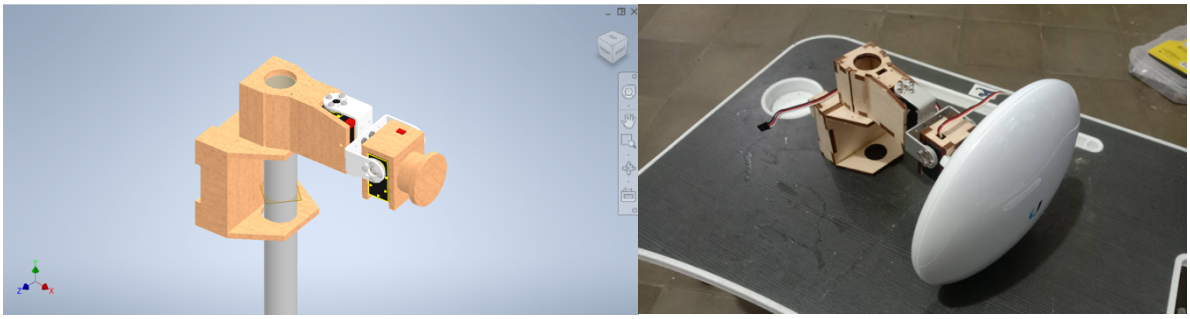

(a) (b)

Figure 41. (a) CAD drawing of the tracker system, (b) Tracker assembled

To transmit the signal optimally, the tracker system is installed on a 1m length aluminum tube with a stand. The tracker connects with the main GCS program to determine the aircraft's position during flight with Ardutracker software that programmed on the microcontroller in the system. Communication between the tracker system and the main GCS is carried out using the mavlink protocol via USB cable connected to the computer. The system's tracker moves with the aircraft to a maximum of 180° on the horizontal axis and 90° on the vertical axis. This movement is sufficient to track the aircraft in the competition area.

7.2.2. Electronic Component Integration

(a) (b) (c) (d)

Figure 42. (a) Mounting for camera, (b) Masking tape and double tape, (c) velcro tape, (d) mounting SBC

A 3D printed mounting is used for the detecting camera. The mounting is made of ABS+ as shown in Figure 42 (a). The components are then adhered to the planes of the fuselage using 3M foam tape and paper tape as shown in Figure 42 (b). To secure the motor x-mounting to the plywood for propulsion purposes, screws are used in each x-mounting holes, as it has been tested in flight test that the plywood has sufficient rigidity to prevent the motor from vibrating. To hold the batteries located in front of the fuselage, a single, high-performance battery strap and velcro are added as shown in Figure 42 (c). Finally, spacers are attached below the SBC and fastened with bolts above it to mount the single board computer used for our mission as shown in Figure 42 (d). Integration of electronic components are discussed further in the following section.

7.3. Electronic Integration

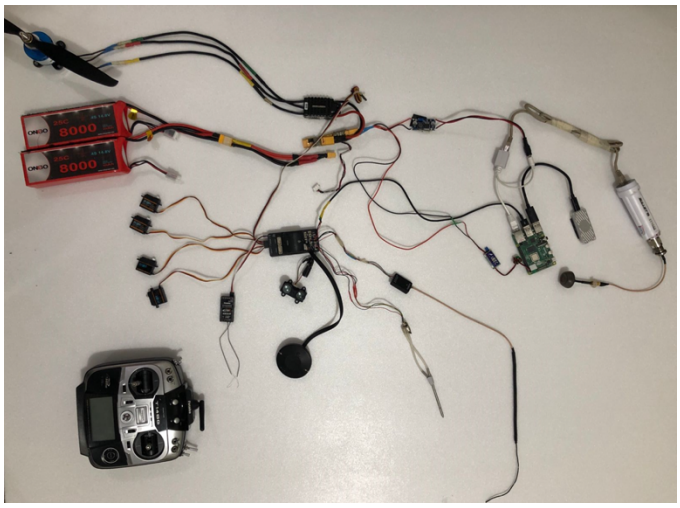

Figure 43. Component integration

The Ashwincarra team's electronics division acts as a selector and determines component specs in the manufacture of a UAV. Where the electronic division begins by consulting with the mechanical division to determine the desired aircraft configuration and performance. Following the discussion, the next step is to choose a motor for the calculation of the thrust-to-weight ratio between the motor and the weight of the aircraft, as well as the required flight time. Furthermore, this step is critical for determining the power loading, which is related to the UAV's maneuvering performance. Typically, we perform calculations using the eCalc application on eCalc.com. The software assists in determining component selection, flight time based on throttle data or average speed, motor efficiency, maximum motor power limit, and other features. In addition, sensor devices such as the FC, ESC, GPS, LIDAR, and computer systems were chosen to support the mission.

Interference in signal frequency, electromagnetic fields generated by the magnetic and electric fields contained in the aircraft, and heat generated by each component must all be considered. With this in mind, it is necessary to position components appropriately to prevent interference between them as detailed in section 7.3.2. UAV Cable Management. Furthermore, the sensors have a high level of sensitivity to outside interference, which affects the UAV's performance. Figure 43 depicts the readiness of electronic integration according to Ashwincarra Teams.

7.3.1. Power Distribution

The primary power source for the system is a 4s2p 8,000mAh Li-Po battery that powers the UAV’s electronics system as shown in Figure 44. Furthermore, the power supply provides enough power to the electronic board and communication module to complete the tasks. According to the Equation 1, flight time is estimated to be 19.8 minutes when powered by a 236,8Wh batteries. Another critical factor to consider is the battery’s C rating. The C Rating of a Li-Po battery indicates its continuous and burst discharge rate. It enables simple calculation of the maximum current that a Li-Po battery safely draws from the battery without causing damage. According to the Equation 7, the ONBO 16,000mAh has a 25-50C 4s2p rating and produce current.

$$Max\ Current\ Draw\ =\ Capactiy\ (Ah)\ x\ C-Rating\ =\ 16\ x\ 25\ =\ 400\ A\quad (7)$$

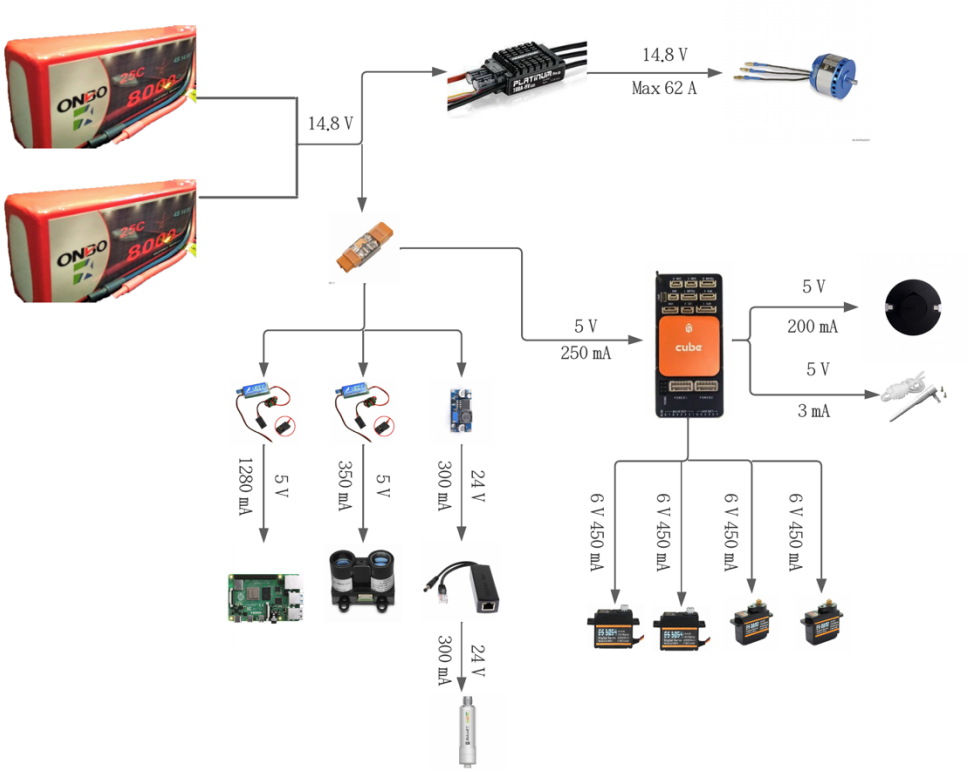

Figure 44. Power distribution for components

7.3.2. UAV Cable Management

In general, the cables on a UAV are arranged in this section by the left side of the aircraft as the power line and the right side as the signal path as shown in Figure 45. The power line contains a current load for a relatively large motor, as well as current for hardware such as FC, SBC, and Wi-Fi. On the right side, there are components that generate signals between components, such as telemetry to the FC, receiver to the FC, Wi-Fi module to the Raspberry Pi, and our antenna, which is set on one side so that it is not affected by the main power line.

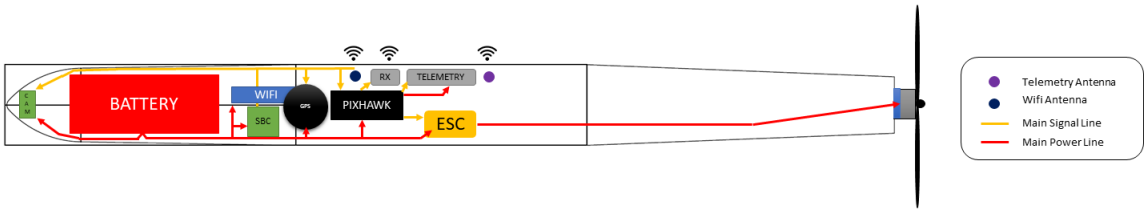

Figure 45. Cable management

The AWG cables are chosen based on the cross-sectional area specifications as well as the length of each cable in order to maintain power and reduce the weight of the aircraft itself. The receiver uses AWG 26 according to the JST-GH connector for flight controller connector wiring, telemetry, and GPS. AWG 22 is used to power the Wi-Fi air and Raspberry Pi from power regulators such as step up (XL6009) and UBEC. AWG 12 cables are then used for cables that function as high-power conductors, such as battery, motor, and ESC. Configuration of the AWG cable is shown in the Table 21.

Table 21. Cable usage

AWG	Usage	Max. Ampere (A)
12	Battery, ESC, Motor, Fuse	9.3
22	Raspberry Pi & Wi-Fi air power supply	0.92
26	Telemetry, Flight Controller, Receiver, Servo	0.457

7.3.3. Reliability and Insulation

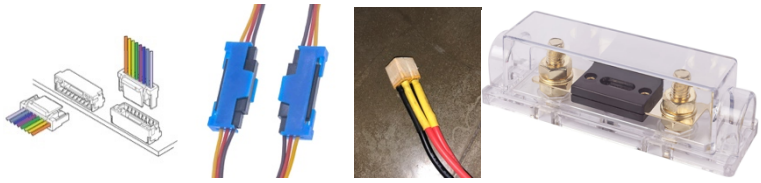

(a) (b) (c) (d)

Figure 46. (a) JST GH connector, (b) Servo lock, (c), XT60 connector, (d) ANL fuse holder

The safety features of each electronic component are important for the safety of the ride itself. Where this section describes the security features used in UAV. The JST GH connector shown in Figure 46 (a) is used as a security measure in several components of the UAV. JST GH is installed on the Pixhawk 2 Cube Orange, telemetry module, and power module, which has the important benefit of a connector with a click that does not easily come off. This is one of the UAV's security features to prevent the cable connector from falling off while in flight. A servo motor is also used as an actuator in the UAV. The servo serves as the primary driver on the control surface, which is the most important component of a UAV. As a result, we add safety to this section by employing a servo lock in Figure 46 (b), which is also light and easy to use. Figure 46 (c) shows heat shrink adhesive attached to soldered cable openings at each end of the connector to strengthen the solder results and avoid shorting the soldered cable openings. And for the overall power connector, use XT60, which is capable of receiving currents of up to 60A continuous and up to 180A when using AWG 12. When an overload ampere occurs, a fuse must be installed toward the current breaker to meet the safety requirements. It is completed with an ANL fuse holder to ensure that the fuse is securely installed and fixed Figure 46 (d).

8. TEST AND SIMULATION

8.1. Sub-System Tests

8.1.1. Simulation Test

In the simulation using the Ansys 2020 R1 software with conditions close to the real situation, several things were obtained that could be reviewed using the Ansys Fluent Fixed Speed method (relative wind speed is always the same in all simulations) based on the condition around the aircraft. Simulations that have been done such as analyzing the total lift and drag, pressure distribution, airflow, and stall condition around the aircraft. Analyzing the forces around the wing area, which is affected by control surface, are included to determine the performance of each control surfaces, compatibility, and safety of control surface servos.

8.1.1.1. Lift, Drag, and Pressure Distribution

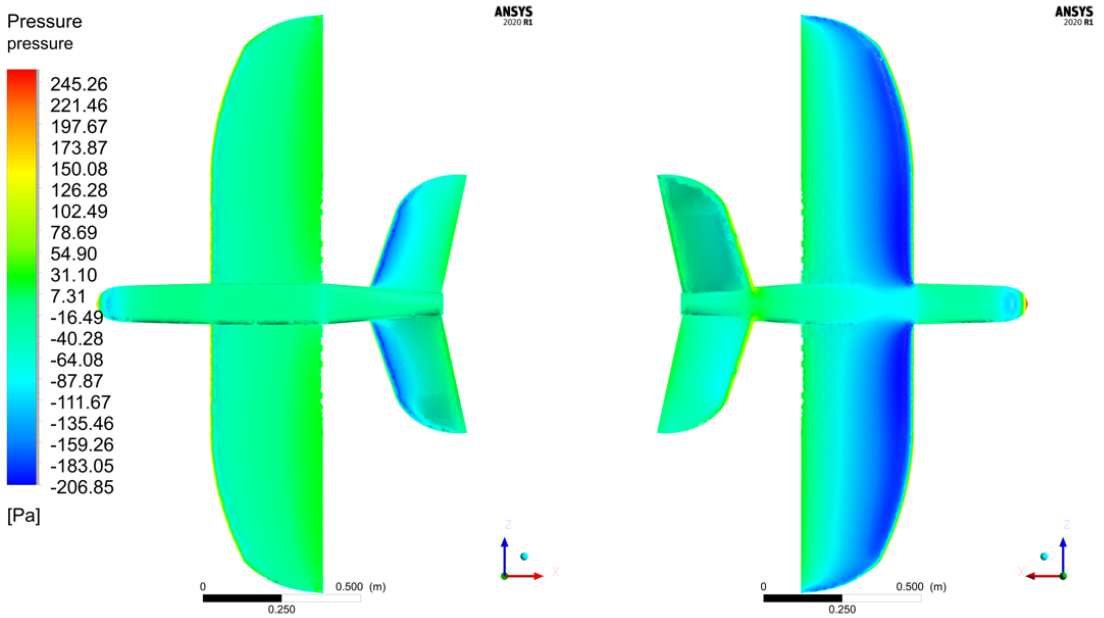

Figure 47. Representation of the pressure distribution from the bottom and the top views of the aircraft

This section explains the results of the final simulation close to the actual condition of the aircraft with the state of 0° AoA and incidence 2° on the wing. Figure 47 explains the contour of pressure distribution at the top and bottom of the aircraft cross section as a whole. Lift and drag forces caused by incidence angle is obtained through simulations. The aircraft has 50.16N of lift force in coefficient of lift about 0.176N and 4.91N of drag force in coefficient of drag about 0.0172.

8.1.1.2. Airflow and Stall Condition

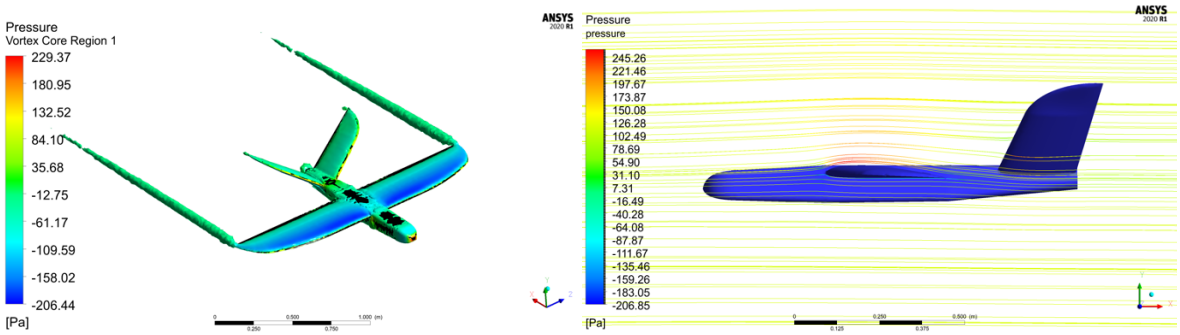

(a) (b)

Figure 48. an overview of the vortex region core and streamline at 0° of AoA (α)

In this section, explanations about airflow and stall condition around the aircraft is added. In Figure 48 the simulation uses cruising condition at 0° AoA (α) and for Figure 48 (a) the airflow condition is simulated using q-criterion method to know pressure distribution for the airflow of every surface on the aircraft. The air vortex is successfully minimized by sharpening the wingtip. While in Figure 48 (b), it shows the airflow from aircraft sided view with its velocity streamline contour.

The simulation is also included for higher angle of attacks until stall condition starts to appear. Stall is a condition where aircraft starts losing lift while pitching up to a higher angle of attack. This condition is usually marked by having flow separation for streamline above and below parts of the aircraft.

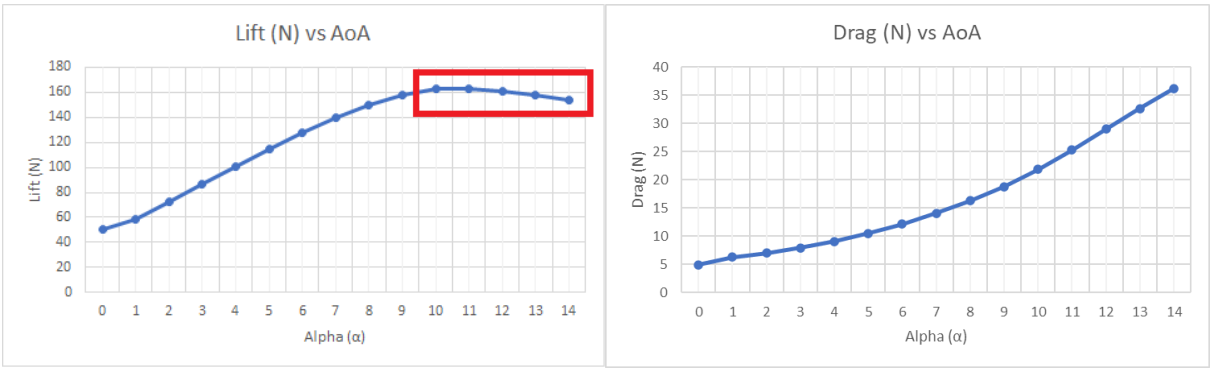

(a) (b)

Figure 49. The simulation results were plotted as a graph of Lift (N) and Drag (N) vs AoA

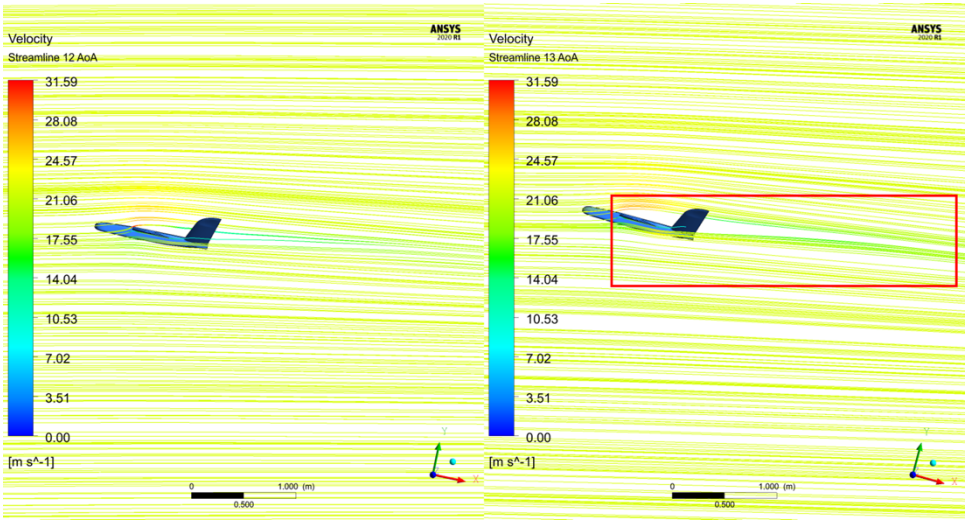

Figure 50. Velocity streamline overview of 12° vs 13° AoA (α)

In Figure 49, there are two graphs showing lift (N) vs AoA and drag (N) vs AoA simulated at a range of 0°-14° AoA. The data gathered in the first table shows that aircraft starts losing lift at 12° AoA and keep losing for higher alpha which is marked by red box inside the graph). As the aircraft losing lift, the drag keeps going higher as seen on the second table. Figure 50 shows a comparison of an airflow between 12° and 13° in a fixed speed method. In Figure 50 on the right side, flow separation starts to occur at 13° AoA which is marked by red box inside the Figure 50.

8.1.1.3. Control Surface Force

In this section, the increase in lift due to the deflection of control surfaces based on simulations approaching the actual condition around the aircraft is explained. The simulations were divided into two parts of the wing affected by the deflection of aileron and ruddervator. The figures also show changes in pressure distribution magnitudes.

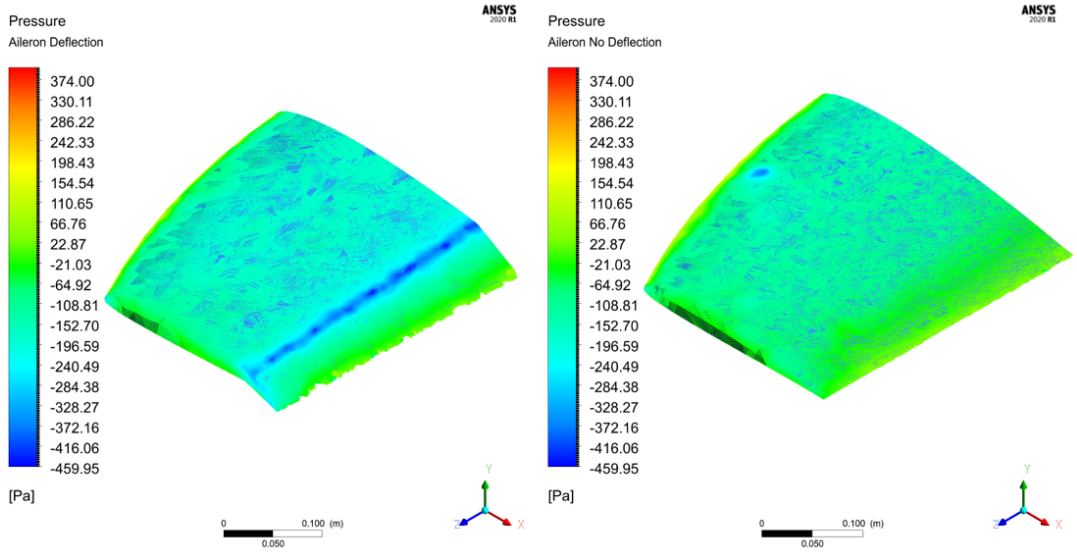

(a) (b)

Figure 51. (a) Lift force on aileron section without deflection, (b) Lift force on aileron section with 20° deflection angle

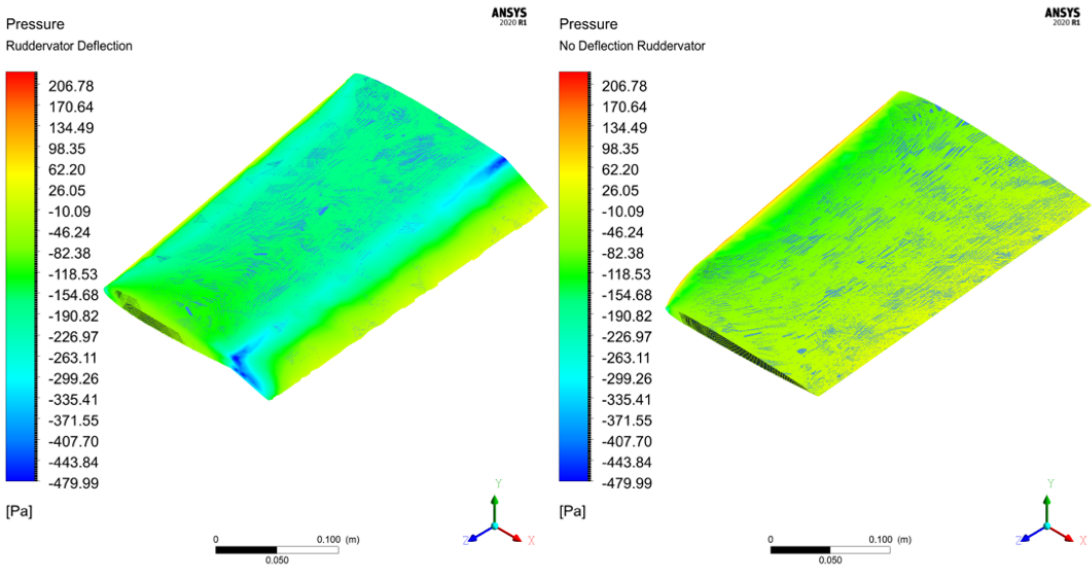

(a) (b)

Figure 52. (a) Lift force on ruddervator section without deflection, (b) Lift force on ruddervator section with 20° deflection angle

Figure 51 shows simulations lift forces on aileron section without and with 20° of deflection angle. Lift force in aileron wing cross-section area without any control surface deflection interference is about 8.33N, and it gets higher in about 20.63N when there is a 20° of deflection angle. The same thing also happens to the lift force in ruddervator stabilizer cross-section area as shown in Figure 52. When there is no deflection angle, the lift force is 0.52N and when there is an addition of 20° deflection angle, the lift force gets up to 15.58N. The increase in the last lift force caused by changes in deflection of each surface control is a benchmark for the actuator to be used.

8.1.2. Wing Load Test

Wing load testing is done by giving an even load on both of the aircraft wings. The load applied to the wing simulates the deformation that occurs in the wing when it gets a force of more than 2G. In this test, 20 plastic bags filled with water weighing about 400 grams each are placed evenly on each wing. The wing deformation is measured using a ruler on the wing tip. The test results show a deformation of 3.5cm when a force of 2.2G is applied to the wing as shown on Figure 53.

(a) (b)

Figure 53. (a) wing load testing, (b) wing deformation measurement

Equation 8 is used to calculate the load factor experienced by the aircraft during flight. This equation is important to know the limit of the aircraft bank angle (Snorri Gudmundsson, 2014).

$$load\ factor = \frac{1}{\cos\theta} \quad (8)$$

The aircraft experienced force around 2G when performing a turning maneuver at a bank angle of 60°. Based on the results of the wing load test, the wing strength is more than sufficient to hold the aircraft. Once the final design is ready, the deformation would be less since the D-Box structure of the wing made out of carbon fiber.

8.1.3. Thrust Test

Thrust test was carried out to determine the actual torque and current ratio of the OS Motor 810KV. Thrust test is carried out with the requirements of digital scales, mounting to attach the motor to be rigid, wattmeter, and receiver. Thrust tests were carried out with the battery configuration installed on the vehicle that 4s2p with a total capacity of 16,000mAh with a propeller size of 13x8-inch. The actual test on Figure 54 (a) and data result on Figure 54 (b).

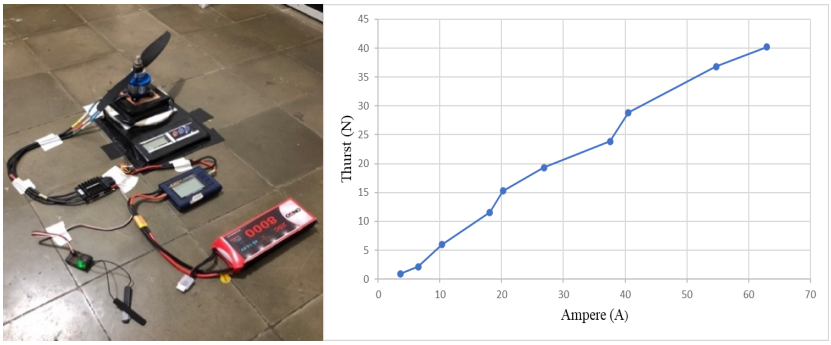

(a) (b)

Figure 54. (a) Thrust test, (b) Graph of thrust vs ampere

8.1.4. Endurance Test

Endurance for an UAV is described at the total time taken during flight. For an electric fixed-wing aircraft is directly related to the capacity of the battery and the amount of the system produces to keep the aircraft in the air.

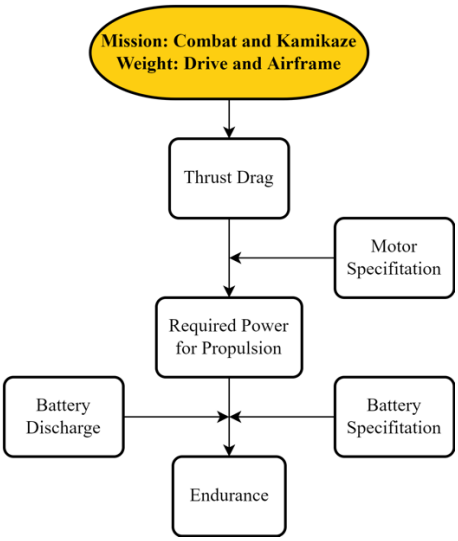

Figure 55. Produce for estimating endurance

There are many other aircraft parameters that determine the endurance for any aircraft as shown in Figure 55, however for simplicity the endurance, calculation is estimated as shown in the Equation 9 below.

$$Endurance(hrs) = \frac{Battery\ Capacity\ (Ah)}{Current\ (A)} \quad (9)$$

The endurance of the aircraft heavily depends on motor specifications, battery specifications, aircraft weight and size. In this case, the endurance test was tested by flying directly with a full system UAV configuration with a target flight time of 20 minutes according to the flight time calculation in the formula above. In this case, the mission for the endurance test is using mission “figure of eight” that there are two desired conditions which are a cruise plane position in straight conditions and a bank maneuver. According to the mission, the throttle is made to fluctuate with the aim of the aircraft in the competition also being able to adjust the throttle with uncertain wind and in order to following opponent plane. The mission shows on Figure 56 and the data result of endurance test show on Table 22.

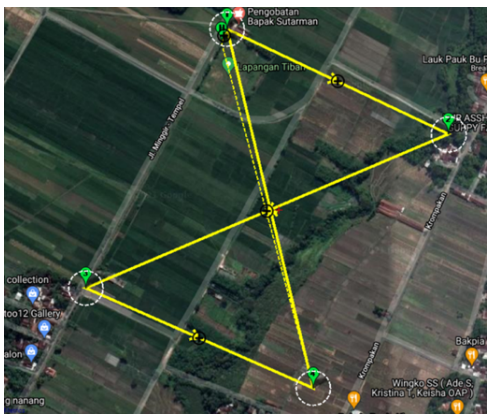

Figure 56. The mission to do endurance test

Table 22. Endurance test

ONBO 8,000mAh 4s2p				
Test	**Flight Time (minutes)**	**Voltage before Flight (V)**	**Voltage after Flight (V)**	**Remain Percentage (%)**
1	16	16,78	15,7	57%
2	20	16,77	15,26	45%
3	25	16,79	15,14	36,5 %

8.1.5. Point to Point Wi-Fi

The results of the Wi-Fi simulation test are portrayed in Figure 57. It displays the simulation with the UAV flying at a distance of over 600m and at an altitude of 100m above the ground. When using a radio Wi-Fi point-to-point connection between the UAV and the ground station, the transfer throughput reaches up to 662Mbps.

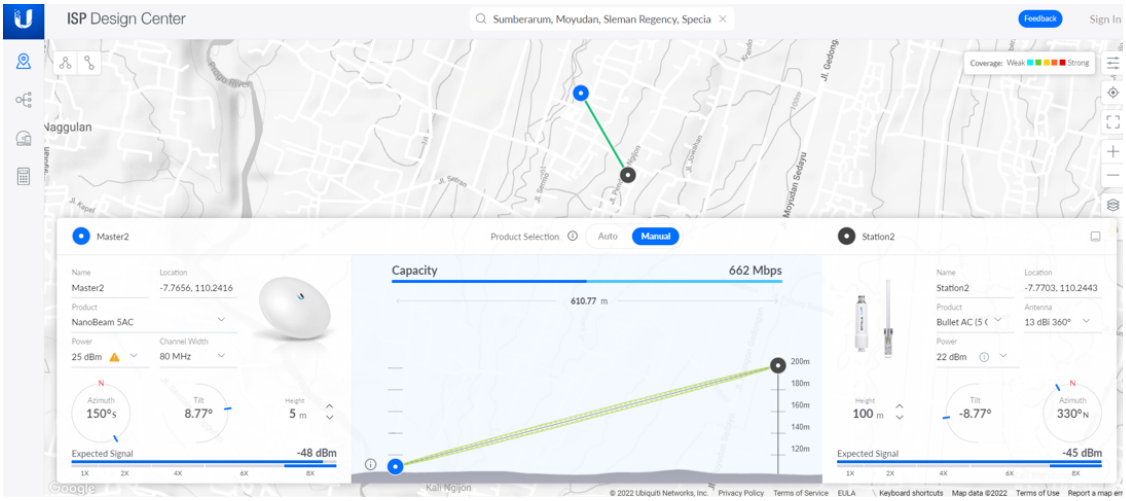

Figure 57. Simulation of Point-to-point Wi-Fi

8.2. Flight Test and Flight Checklist

8.2.1. Flight Checklist

In this section, we provide the team's standard operating procedure which contains preflight checklist from each unit as shown in Figure 58.

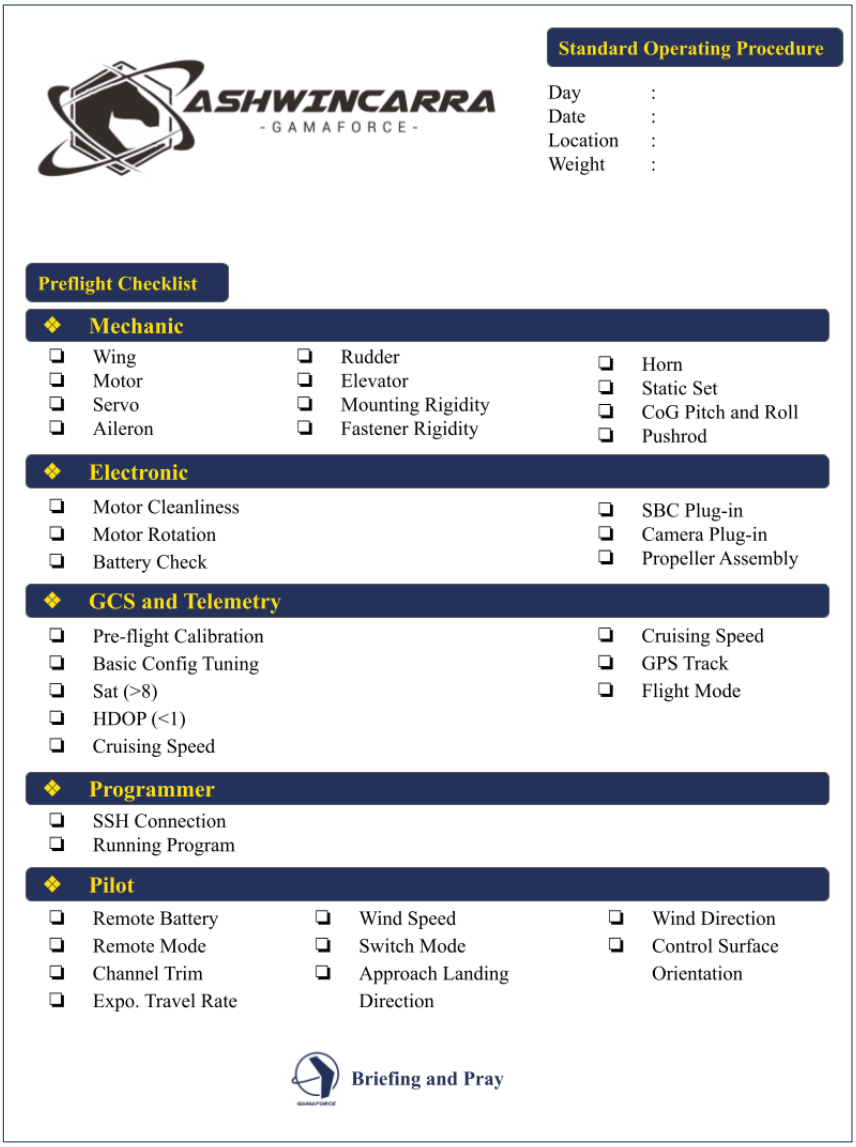

ASHWINCARRA
- GAMAFORCE -

Standard Operating Procedure

Day :
Date :
Location :
Weight :

Preflight Checklist

❖ Mechanic

- ❑ Wing
- ❑ Motor
- ❑ Servo
- ❑ Aileron
- ❑ Rudder
- ❑ Elevator
- ❑ Mounting Rigidity
- ❑ Fastener Rigidity
- ❑ Horn
- ❑ Static Set
- ❑ CoG Pitch and Roll
- ❑ Pushrod

❖ Electronic

- ❑ Motor Cleanliness
- ❑ Motor Rotation
- ❑ Battery Check
- ❑ SBC Plug-in
- ❑ Camera Plug-in
- ❑ Propeller Assembly

❖ GCS and Telemetry

- ❑ Pre-flight Calibration
- ❑ Basic Config Tuning
- ❑ Sat (>8)
- ❑ HDOP (<1)
- ❑ Cruising Speed
- ❑ Cruising Speed
- ❑ GPS Track
- ❑ Flight Mode

❖ Programmer

- ❑ SSH Connection
- ❑ Running Program

❖ Pilot

- ❑ Remote Battery
- ❑ Remote Mode
- ❑ Channel Trim
- ❑ Expo. Travel Rate
- ❑ Wind Speed
- ❑ Switch Mode
- ❑ Approach Landing Direction
- ❑ Wind Direction
- ❑ Control Surface Orientation

Briefing and Pray

Figure 58. Ashwincarra's Standard Operating Procedure

8.2.2. Autopilot Test

Missions such as auto-takeoff and auto-landing are prioritized during the autopilot test, along with Geofence, fail safe, and ardutracker parameters. Figure 59 depicts the documentation of autopilot test.

(a) (b) (c)

Figure 59. (a) The UAV, (b) Pre-flight, (c) Post-flight

8.2.2.1. Geofence

Geofencing in Ardupilot allows the UAV to set a virtual 'fence' around the area of the UAV want to fly in, specified as an enclosed polygon of GPS positions plus a minimum and maximum altitude. When fencing is enabled, if a plane goes outside the fenced area, then it is going to switch to guided mode and will fly back to a pre-defined return point and loiter there ready to be taken over by the pilot.

8.2.2.2. Auto Take-Off & Landing

Figure 60. Hand launch take-off

To meet mission requirement, Ashwincarra team do auto take-off to start the mission and landing to end the mission. Ashwincarra team uses the hand launch method to perform auto take-off mode as shown in Figure 60. The auto take-off mode uses the acceleration parameter of the GPS displacement. For landing mode assisted with LIDAR to get an accurate altitude. All parameters of auto take-off and landing need practice and find the best parameters.

8.2.2.3. Ardutracker

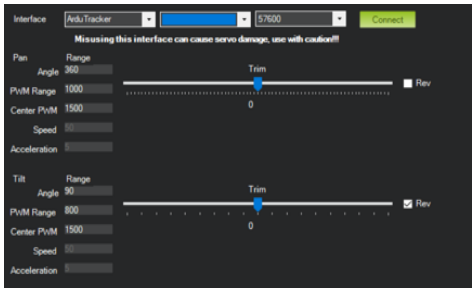

Figure 61. Ardutracker

One of methods to get the best connectivity for our Wi-Fi communication is using an antenna tracker. Antenna tracker serves to direct the Wi-Fi ground to the UAV which is always moving dynamically using Ardutracker feature on Mission Planner software as shown in Figure 61. With this help, it optimizes the connection between Wi-Fi signals.

8.2.2.4. Fail Safe Test

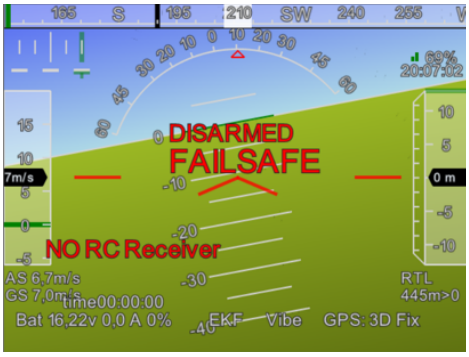

Figure 62. Fail safe test

Fail safe on UAV is useful to avoid an accident to the environment. Fail safe is activated when the Remote Control (RC) is out of range and other UAV fails as shown in Figure 62 so it improves security features. In addition, the flight termination software is made for emergency conditions (communication loss and UAV departs the flight area) for more than 10 seconds. The software on the on-board computer orders the UAV to perform throttle cutting, full pitch up, full right rudder and aileron by transmitting the PWM value to the FC.

8.2.3. Autonomous Mission Test

8.2.3.1. Autonomous Lockdown Test

Multiple stages of autonomous lockdown testing are conducted, including detection testing, autonomous tracking control testing, and centering control testing. Table 23 describes the preparedness of the subtest, and Figure 63 shows the result of the detection test.

Table 23. Testing result of autonomous lockdown

Sub-test	Progress
Detection	Successfully detects UAV.
Tracking control	Successfully guide the UAV to waypoints and adjust the speed with PID controller.
Centering control	Successfully control the actuator based on the PWM value calculated by PID controller using video as input.

Figure 63. Detection test result

8.2.3.2. Kamikaze Test

Figure 64. Kamikaze test

The kamikaze mission was tested on a 2x2m printed QR-code, but it did not provide a cover panel as required by the competition. In general, this mission's software is successful. Based on tests, our UAV needs dive to 9 meters on altitude with a 50° pitch angle. This software will be improved on the speed of QR-code detection in order to avoid the UAV from diving too low and the risk of crash. In addition, cover panels will be added for the subsequent tests. Figure 64 is the result of the QR-code detection with the message "ASHWINCARRA_ID".

9. SAFETY

Safety is the prime priority during both flight tests and competitions. As a result, we prepare first aid kit, Li-Po Bag, and safety equipment as prevention kits as explained in Table 24.

Table 24. Safety equipment

Prevention kits	Explanation
First Aid Kit 	Provided first aid kit box that can hold supplies used to treat minor injuries including cuts, scrapes, burns, bruises, and sprains which are caused by accident in the area competition.
Li-Po Bag 	Li-Po Bag is used to keep Li-Po Batteries for its safety needs. Li-Po bag is an absolute necessity during travel. Due to the flammable nature of lithium chemistry batteries, several airlines demand the use of flame-resistant storage and charging bags.
Safety Equipment while testing the UAV 	To maximize our launcher safety by using a hand-launch method, safety equipments are used such as gloves, protective helmet, safety vest, and goggles.

10. REFERENCES

Babenko, B., Belongie, S. and Yang, M.H. (2009), "Visual tracking with online multiple instance learning", *2009 IEEE Conference on Computer Vision and Pattern Recognition, CVPR 2009*, IEEE, pp. 983–990.

eCalc. (2022), "eCalc-Online propeller calculator", Available at : http://www.ecalc.ch.

Henriques, J.F., Caseiro, R., Martins, P. and Batista, J. (2015), "High-speed tracking with kernelized correlation filters", *IEEE Transactions on Pattern Analysis and Machine Intelligence*, Vol. 37 No. 3, pp. 583–596.

Kim, J.A., Sung, J.Y. and Park, S.H. (2020), "Comparison of Faster-RCNN, YOLO, and SSD for Real-Time Vehicle Type Recognition", *2020 IEEE International Conference on Consumer Electronics - Asia, ICCE-Asia 2020*, pp. 0–3.

L. Hudson. (2022) 'Pyzbar: Read One-Dimensional Barcodes and QR Codes from Python 2 and 3', Python Library Version 0.1.9. *Available at* : https://github.com/NaturalHistoryMuseum/pyzbar/.

Liu, W., Anguelov, D., Erhan, D., Szegedy, C., Reed, S., Fu, C. Y., and Berg, A. C. (2016), "SSD : Single Shot MultiBox Detector", *Springer International Publishing*, pp. 21-37.

Lukežič, A., Vojíř, T., Čehovin Zajc, L., Matas, J. and Kristan, M. (2018), "Discriminative Correlation Filter Tracker with Channel and Spatial Reliability", *International Journal of Computer Vision*, Vol. 126 No. 7, pp. 671–688.

Quigley, Morgan, et al. (2009) 'ROS : an open-source Robot Operating System', *2009 IEEE International Conferences on Robotics and Automation Workshop on Open Source Software.*

Raymer, D. (2018), "Aircraft Design: A Conceptual Approach, Sixth Edition", *Aircraft Design: A Conceptual Approach, Sixth Edition*, available at:https://doi.org/10.2514/4.104909.

Redmon, J., Divvala, S., Girshick, R. and Farhadi, A. (2016), "You only look once: Unified, real-time object detection", *Proceedings of the IEEE Computer Society Conference on Computer Vision and Pattern Recognition*, Vol. 2016-December, IEEE Computer Society, pp. 779–788.

Ren, S., He, K., Girshick, R. and Sun, J. (2017), "Faster R-CNN: Towards Real-Time Object Detection with Region Proposal Networks", *IEEE Transactions on Pattern Analysis and Machine Intelligence*, IEEE Computer Society, Vol. 39 No. 6, pp. 1137–1149.

Rosebrock, Adrian. (2018), *"Simple object tracking with OpenCV"* Available at : https://pyimagesearch.com/2018/07/23/simple-object-tracking-with-opencv/.

Roskam, J. (2003), "Airplane Aerodynamics and Performance - Jan Roskam.pdf".

Sanchez-Carmona, A. And Cuerno-Rejado, C. (2019), "Vee-tail conceptual design criteria for commercial transport aeroplanes", *Chinese Journal of Aeronautics*, Chinese Society of Aeronautics and Astronautics, Vol. 32 No. 3, pp. 595–610.

Sandler, M., Howard, A., Zhu, M., Zhmoginov, A. and Chen, L.C. (2018), "MobileNetV2: Inverted Residuals and Linear Bottlenecks", *Proceedings of the IEEE Computer Society Conference on Computer Vision and Pattern Recognition*, IEEE, pp. 4510–4520.

Selig, M.S., Guglielmo, J.J., Broeren, A.P. and Giguère, P. (1995), *Summary of Low Speed Airfoil Dara - Vol 1*, *Uicc*, Vol. 1.

Snorri Gudmundsson. (2014), *General Aviation Aircraft Design : Applied Methods*.

Wu, J., Leng, C., Wang, Y., Hu, Q. and Cheng, J. (2016), "Quantized convolutional neural networks for mobile devices", *Proceedings of the IEEE Computer Society Conference on Computer Vision and Pattern Recognition*, IEEE, Vol. 2016-Decem, pp. 4820–4828.

Xiong, Y., Liu, H., Gupta, S., Akin, B., Bender, G., Wang, Y., Kindermans, P.J., *et al.* (2021), "MobileDets: Searching for Object Detection Architectures for Mobile Accelerators", *Proceedings of the IEEE Computer Society Conference on Computer Vision and Pattern Recognition*, IEEE, pp. 3824–3833.